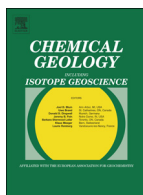




Contents lists available at ScienceDirect



Chemical Geology

journal homepage: www.elsevier.com/locate/chemgeo

1 Highlights

2 **Fingerprints of metamorphism in chromite: New insights from minor and**
3 **trace elements**4 *Chemical Geology xxx (2014) xxx–xxx*5 **Vanessa Colás ^{a,b,*}, José M. González-Jiménez ^{b,c}, William L. Griffin ^b, Isabel Fanlo ^a, Fernando Gervilla ^d, Suzanne Y. O'Reilly ^b, Norman J. Pearson ^b, Thomas Kerestedjian ^e, Joaquín A. Proenza ^f**6 ^a Universidad de Zaragoza, Departamento de Ciencias de la Tierra, Pedro Cerdanya 12, 50009 Zaragoza, Spain7 ^b ARC Centre of Excellence for Core to Crust Fluid Systems (CCFS), GEMOC National Key Centre, Department of Earth and Planetary Sciences, Macquarie University, Sydney, NSW 2109, Australia9 ^c Departamento de Geología, Andean Geothermal Center of Excellence (CEGA), Universidad de Chile, Santiago, Chile10 ^d Departamento de Mineralogía y Petrología and Instituto Andaluz de Ciencias de la Tierra (Universidad de Granada-CSIC), Facultad de Ciencias, Avda. Fuentenueva, s/n, 18002 Granada, Spain11 ^e Geological Institute, Bulgarian Academy of Sciences, 24 Georgi Bonchev Str., 1113 Sofia, Bulgaria12 ^f Departament de Cristallografia, Mineralogia i Dipòsits Minerals, Facultat de Geologia, Universitat de Barcelona, Martí i Franquès, s/n, 08028 Barcelona, Spain13

- Metamorphism has produced different microstructures in chromites.
- Microstructural changes in chromite also involve variations of minor- and trace-elements.
- Interaction between cores and surrounding rims could modify the original composition.
- LA-ICP-MS analysis may reveal fingerprints of metamorphism in chromite.

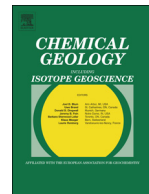
Appendix A Digital dataset of electron-microprobe analysis of chromite from studied [chromitites](#) of the Metamorphic Rhodope Complex (Bulgaria) and the ophiolites of New Caledonia (Dyne) and Cuba (Mercedita).

Appendix B Results of repeated analyses of the BCR-2g and LCR-1 standard by laser ablation ICP-MS (New Wave UP 266) and comparison with literature values.

Appendix C Dataset of LA-ICP-MS analysis of minor and trace elements in chromite from studied [chromitites](#) of the Metamorphic Rhodope Complex (Bulgaria) and the ophiolites of New Caledonia (Dyne) and Cuba (Mercedita).



Contents lists available at ScienceDirect



Chemical Geology

journal homepage: www.elsevier.com/locate/chemgeo

1 Fingerprints of metamorphism in chromite: New insights from minor 2 and trace elements

1 **Vanessa Colás^{a,b,*}, José M. González-Jiménez^{b,c}, William L. Griffin^b, Isabel Fanlo^a, Fernando Gervilla^d,**
2 **Suzanne Y. O'Reilly^b, Norman J. Pearson^b, Thomas Kerestedjian^e, Joaquín A. Proenza^f**

3 ^a Universidad de Zaragoza, Departamento de Ciencias de la Tierra, Pedro Cerbuna 12, 50009 Zaragoza, Spain

4 ^b ARC Centre of Excellence for Core to Crust Fluid Systems (CCFS), GEMOC National Key Centre, Department of Earth and Planetary Sciences, Macquarie University, Sydney, NSW 2109, Australia

5 ^c Departamento de Geología, Andean Geothermal Center of Excellence (CEGA), Universidad de Chile, Santiago, Chile

6 ^d Departamento de Mineralogía y Petrología and Instituto Andaluz de Ciencias de la Tierra (Universidad de Granada-CSIC), Facultad de Ciencias, Avda. Fuentenueva, s/n, 18002 Granada, Spain

7 ^e Geological Institute, Bulgarian Academy of Sciences, 24 Georgi Bonchev Str., 1113 Sofia, Bulgaria

8 ^f Departament de Cristallografia, Mineralogia i Dipòsits Minerals, Facultat de Geologia, Universitat de Barcelona, Martí i Franquès, s/n, 08028 Barcelona, Spain

1 1 ARTICLE INFO

12 Article history:

13 Received 8 April 2014

14 Received in revised form 1 October 2014

15 Accepted 2 October 2014

16 Available online xxxx

17 Editor: L. Reisberg

18 Keywords:

19 Chromite

20 Metamorphism

21 Laser-ablation ICP-MS

22 Mobility of minor and trace element

23 Rhodope metamorphic complex

1 1 ABSTRACT

24 A suite of minor and trace elements (Ga, Ti, Ni, Zn, Co, Mn, V, Sc) in chromite grains from ophiolitic chromitites subjected to high-pressure metamorphism defines a metamorphic signature. A two-stage process associated with the infiltration of fluids during retrograde metamorphism from eclogite- to amphibolite-facies has produced four types of chromites: (1) porous chromite strongly enriched in Cr and Fe^{2+} but depleted in Al and Mg, with abundant chlorite filling the pores; (2) non-porous chromite strongly enriched in Fe^{3+} (i.e., ferrian chromite); (3) partly altered chromite with primary cores surrounded by chlorite-bearing porous chromite; and (4) zoned chromite made up of primary cores surrounded by non-porous rims of ferrian chromite. Compared to spinels from unmetamorphosed chromitites the cores of partly altered chromites after primary high-Cr chromite are enriched in Zn, Co and Mn but strongly depleted in Ga, Ni and Sc. This distribution of minor- and trace-elements is related to a decrease in Mg# [$Mg/(Mg + Fe^{2+})$] and Al, produced by the crystallization of chlorite in the pores of porous chromite. Non-porous chromite is enriched in Ti, Ni, Zn, Co, Mn and Sc but depleted in Ga, suggesting that fluid-assisted processes have obliterated the primary magmatic signature. Zoned chromites have cores depleted in Ga, Ni and Sc but are progressively enriched in Zn, Co and Mn as Mg# and Al decrease toward the rims; they have overall lower concentrations in Ga, Ni and Sc and higher Zn and Co than the non-porous rims of ferrian chromite. The complex variation of the minor- and trace-elements vs Fe^{3+} / Fe^{2+} in the different types of chromite suggests a complex interplay of substitutions, linked with the ability of fluids to infiltrate the chromite and the extent of the re-equilibration between pre-existing cores and newly-formed rims.

The results demonstrate that metamorphism can seriously disturb the original magmatic distribution of minor and trace elements in chromite. The abundances of these elements, and by inference the major elements, can be strongly modified even in the cores of grains that appear "unaltered" in terms of major elements. The use of the major elements as indicators of magmatic processes therefore must be linked to careful evaluation of metamorphic effects, using LA-ICP-MS analysis of minor and trace elements.

48 © 2014 Published by Elsevier B.V.

49

50

51

52 1. Introduction

53 Chromite is an oxide with a spinel-type structure that might be expressed using the general formula AB_2O_4 . The A site is occupied by Mg and Fe^{2+} in tetrahedral coordination and the B site is usually

54 occupied by Cr and Al in octahedral coordination; Cr and Al may be substituted by Fe^{3+} giving rise to ferrian chromite. Elements like Zn^{2+} , Co^{2+} , Mn^{2+} and Ni^{2+} can substitute Mg and Fe^{2+} in A and V^{3+} , Sc^{3+} , Ga^{3+} and Ti^{4+} can substitute Al and Cr in B (Table 1). These variations in the composition of chromite are commonly used to interpret the petrogenesis and the geodynamic setting of the host ultramafic rocks (Irvine, 1967; Dick and Bullen, 1984; Arai, 1992; Stowe, 1994; Zhou and Robinson, 1994; Barnes and Roeder, 2001; Kamenetsky et al., 2001; Ahmed et al., 2005; Rollinson, 2008; Pagé and Barnes, 2009). The high resistance of chromite to alteration (compared to the primary silicates) has made this oxide particularly useful as a petrogenetic indicator in ultramafic rocks in which metamorphic

* Corresponding author at: Universidad de Zaragoza, Departamento de Ciencias de la Tierra, Pedro Cerbuna 12, 50009 Zaragoza, Spain. Tel.: +34 976 84 10 98.

E-mail addresses: vcolas@unizar.es (V. Colás), jose.gonzalez@mq.edu.au, jmgonzj@ing.uchile.cl (J.M. González-Jiménez), bill.griffin@mq.edu.au (W.L. Griffin), fanlo@unizar.es (I. Fanlo), gervilla@ugr.es (F. Gervilla), sue.oreilly@mq.edu.au (S.Y. O'Reilly), norman.pearson@mq.edu.au (N.J. Pearson), thomas.kerestedjian@gmail.com (T. Kerestedjian), japroenza@ub.edu (J.A. Proenza).

Table 1

Major-, minor- and trace element distribution in the different mineral structures.

	Chromite		Olivine	Chlorite
Formula	AB_2O_4		A_2SiO_4	$(A_5Al)(Si_3Al)O_{10}(OH)_8$
Position	$A^{(IV)}$	$B^{(VI)}$	$A^{(VI)}$	$A^{(VI)}$
Major elements	Mg^{2+}, Fe^{2+}	$Cr^{3+}, Al^{3+}, Fe^{3+}$	Mg^{2+}, Fe^{2+}	Mg^{2+}, Fe^{2+}
Minor- and trace elements	$Zn^{2+}, Co^{2+}, Mn^{2+}, Ni^{2+}$	$V^{3+}, Sc^{3+}, Ga^{3+}, Ti^{4+}$	$Zn^{2+}, Co^{2+}, Mn^{2+}, Ni^{2+}$	Ni^{2+}

alteration has obliterated other primary fingerprints (e.g. Proenza et al., 2004; Ahmed et al., 2005; González Jiménez et al., 2009). However, a growing body of work, based on the study of chromite-rich rocks from ophiolites, layered complexes and komatiites, has shown that the chemistry and structure of chromite can be also significantly modified during both prograde (Bliss and MacLean, 1975; Evans and Frost, 1975; Wylie et al., 1987; Frost, 1991; Burkhard, 1993; Abzalov, 1998; Barnes, 2000; González Jiménez et al., 2009; Merlini et al., 2009; Olobaniyi and Mücke, 2011) and retrograde **metamorphisms** (Loferski, 1986; Proenza et al., 2004, 2008; Mellini et al., 2005; Mukherjee et al., 2010; Gervilla et al., 2012; Grieco and Merlini, 2012).

Metamorphism typically imposes an optical and chemical zoning on the primary chromite. In general, a zone enriched in FeO and Cr_2O_3 and depleted in MgO and Al_2O_3 surrounds the apparently pristine (or primary) core, which grades outwards to chromite strongly enriched in Fe^{3+} (ferrian chromite) (Bliss and MacLean, 1975; Evans and Frost, 1975; Wylie et al., 1987; Kimball, 1990; Barnes, 2000; Mellini et al., 2005; González Jiménez et al., 2009; Merlini et al., 2009; Mukherjee et al., 2010; Gervilla et al., 2012; Grieco and Merlini, 2012). Occasionally magnetite rims surround the cores and/or the ferrian chromite rims.

Evans and Frost (1975), Bliss and MacLean (1975) and Barnes (2000) have suggested that the ferrian chromite is produced by the reaction of pristine cores with magnetite rims during prograde metamorphism of serpentinised ultramafic rocks. In contrast, Gervilla et al. (2012) proposed that the formation of ferrian chromite is a two-stage process occurring during the retrograde evolution of chromites from eclogite-facies conditions. During the first stage, magmatic chromite reacts with olivine in the presence of reducing fluids to produce a porous chromite enriched in FeO and Cr_2O_3 (hereafter Fe^{2+} -rich chromite), which is in equilibrium with chlorite. In the second stage, **oxidizing** solutions circulate through the network of pores in the porous chromite, dissolving chlorite and adding Fe^{3+} , which diffuses into the chromite lattice and converts it to ferrian chromite (i.e., Fe^{3+} -rich chromite).

Both models implicitly assume that the cores of chromite grains represent relict primary chromite that remained unaffected by the alteration. However, the selective enrichment of a suite of minor elements including Mn, Ni, Co, Zn and Ti in such “pristine cores”, in metamorphosed chromites from the Tidding Suture Zone in the eastern Himalaya (Singh and Singh, 2013) and the Nuggihalli schist belt in India (Mukherjee et al., 2010) led us to investigate whether their compositions are perturbed and do not represent original pristine compositions. If so, important information about the metamorphic evolution of chromite might be lost by **analyzing** only microstructures and the abundances of major elements, and deductions about the original magmatic-tectonic situation of the chromitites and their host peridotites might be incorrect.

The technique of laser-ablation inductively-coupled plasma-mass spectrometry (LA-ICP-MS) has lower limits of detection than the electron microprobe and thus can **analyze** a more comprehensive suite of elements present in a chromite ($Ga, Ti, Ni, Zn, Co, Mn, V$ and Sc), providing useful information about its **petrogenesis** (Dare et al., 2009; Pagé and Barnes, 2009; González-Jiménez et al., 2011, 2013, 2014; Aldanmaz, 2012). In this work LA-ICP-MS was used to measure the minor- and trace elements in highly metamorphosed chromites, in order to define the fingerprints of metamorphism that are not revealed by conventional

approaches based on electron microprobe data. We have studied chromite from metamorphosed chromitites because they preserve zoning patterns better than accessory chromites in peridotite at a given degree of alteration (e.g. Proenza et al., 2004). The chromitites are enclosed in four ultramafic massifs (Golyamo Kamenyane, Chernichevo, Yakovitsa and Avren) representing portions of the dismembered ophiolites of the Rhodope Metamorphic Core Complex in southern Bulgaria. The chromitites and their host ultramafic rocks underwent metamorphism in eclogite facies with a later amphibolite-facies overprint (Mposkos and Krohe, 2000, 2006; Mposkos, 2002; Mposkos et al., 2011). In order to test the validity of our approach we have additionally compared our chromites with those from unaltered chromitites in unmetamorphosed ophiolites (Eastern Cuba and New Caledonia) with well-documented post-magmatic histories.

2. Sample background

The samples selected for this study are from Type I ophiolitic chromitites (i.e., enriched in IPGE relative to PPGE; González-Jiménez et al., 2014) in the metamorphosed ultramafic massifs of Golyamo Kamenyane, Chernichevo, Yakovitsa and Avren in the eastern part of the Rhodope Metamorphic Core Complex, of southern Bulgaria and northern Greece (Table 2 and Fig. 1).

The Rhodope Metamorphic Core Complex is a large domal structure formed mainly during the Alpine orogeny; it lies between the Balkan belt to the north and the Dinarides–Hellenides to the south-southwest (Fig. 1). The complex consists of (1) a lower unit corresponding to the autochthonous core and known as the Gneiss–Migmatite Complex (Kozhoukharov et al., 1988; Haydoutov et al., 2001), the lower High-Grade Unit (Bonev, 2006) or the Lower Allochthon (Janák et al., 2011), and (2) an upper unit with meta-ophiolites (Kolcheva and Eskenazy, 1988; Bazylev et al., 1999; Kolcheva et al., 2000; Haydoutov et al., 2001, 2004; Bonev et al., 2006; Daieva et al., 2007) which represents the allochthonous rim and is known as the variegated complex (Kozhoukharov et al., 1988; Haydoutov et al., 2001), the upper High-Grade Unit (Bonev, 2006) or the Upper Allochthon (Janák et al., 2011). In the eastern part of the Rhodope Metamorphic Core Complex, both the autochthonous core and the allochthonous rim crop out in two large-scale domal structures: the Kesebir–Kardamis Dome to the west and the Byala Reka–Kechros Dome to the east (Fig. 1; Georgiev, 2006).

The ultramafic massifs of Golyamo Kamenyane, Avren, and Chernichevo crop out in the western limb of the Byala Reka–Kechros Dome along the Avren synform (Fig. 1). The ultramafic massif of Yakovitsa crops out in the western limb of the Kesebir–Kardamis Dome (Fig. 1). These ultramafic massifs consist of partly serpentinised harzburgite and dunite, which are overlain by layers of amphibolites (i.e. formerly layered gabbros; Bazylev et al., 1999; Kolcheva et al., 2000; Haydoutov et al., 2004; Gervilla et al., 2012) in the massifs of Golyamo Kamenyane and Chernichevo. These lithologies, including chromitites, are cut by sub-vertical veins of asbestos, mainly anthophyllite and chrysotile, and talc in the massifs of Golyamo Kamenyane (Gervilla et al., 2012) and Avren (Kolkovski et al., 2003).

Mposkos and Krohe (2000, 2006) and Mposkos (2002) investigated spinel-garnet metaperidotites and garnet pyroxenites of the Kimi Complex (the Greek equivalent of the Avren synform in Bulgaria) and concluded that the mantle rocks of the allochthonous rim of the

t2.1
t2.2
t2.3
t2.4
t2.5
t2.6
t2.7
t2.8
t2.9
t2.10
t2.11
t2.12
t2.13
t2.14
t2.15
t2.16
t2.17
t2.18
t2.19
t2.20
t2.21
t2.22
t2.23
t2.24
t2.25
t2.26
t2.27
t2.28
t2.29
t2.30
t2.31
t2.32
t2.33
t2.34
t2.35

Table 2
Characterization of the chromitite samples investigated in this study.

Locality	Sample	Size of the body (wide)	Location in the chromitite body	Texture	Chromite microstructure	Chromite grain zone	Chemical Variations		
							Cr#	Mg#	Fe ³⁺ /(Fe ³⁺ + Fe ²⁺)
<i>High-Al Chromitites</i>									
Golyamo Kamenyane	GK1A-5	>10 m	Core	Semimassive	Partly altered chromite	Core	0.52–0.60	0.59–0.71	<0.30
	GK1A-6								
	GK1A-7								
	GK3C-1					Porous rim	0.57–0.91	0.44–0.68	<0.28
	GK3-100								
	GK3-101								
	GK4-100								
	GK1A-4	>10 m	Core	Semimassive	Porous chromite	Core to rim profile	0.91–0.96	0.35–0.48	0.21–0.53
	GK3A-1								
	GK1C-3	>10 m	Shear zone	Massive	Zoned chromite	Core	0.62–0.69	0.49–0.57	0.10–0.34
						Non-porous rim	0.83–0.99	0.20–0.36	0.49–0.63
	GK1C-1	>10 m	Shear zone	Massive	Non-porous chromite	Core to rim profile	0.96–0.99	0.16–0.32	0.55–0.66
	GK1C-2								
Chernichevo	CH1-4	>1 m	Core	Semimassive	Partly altered chromite	Core	0.55	0.59	0.31
						Porous rim	0.58–0.65	0.51–0.57	0.27–0.32
<i>High-Cr Chromitites</i>									
Yakovitsa	J1-H1	30–40 cm	Core	Massive	Partly altered chromite	Core	0.71–0.78	0.59–0.69	0.07–0.26
	J1-E2								
	J1-B7		Core			Porous rim	0.78–0.97	0.45–0.66	0.18–0.43
	J1-B6		Rim						
	J1-B2								
	J1-D1	20–30 cm	Core	Disseminated	Partly altered chromite	Core	0.60–0.83	0.40–0.65	0.05–0.29
	J1-F1					Porous rim	0.78–0.98	0.29–0.46	0.31–0.50
	J1-G2								
	J1-A3	<20 cm	Core	Disseminated	Zoned chromite	Core	0.68–0.73	0.38–0.42	0.08–0.17
						Non-porous rim	0.91–0.98	0.16–0.27	0.43–0.61
Avren	AV3-117	1–2 m	Core	Massive	Zoned chromite	Core	0.84–0.93	0.35–0.46	0.19–0.31
	AV3-110		Core & Rim	Semimassive					
	AV3								
	AV3-121		Rim	Disseminated		Non-porous rim	0.93–0.98	0.08–0.35	0.50–0.67

179 Complex have undergone ultra-high pressure (UHP)/high temperature
180 (HT) metamorphism (>25 kbar and >200 °C), and a later overprinting
181 in eclogite- or granulite-facies (13.5–16 kbar and 750–775 °C). An
182 amphibolite-facies (~10 kbar and 600–650 °C) overprint is also recorded
183 in metasediments spatially associated with the mantle rocks (Mposkos
184 and Krohe, 2000, 2006; Mposkos, 2002). Mposkos et al. (2011) have es-
185 timated a somewhat similar retrograde metamorphic pathway in the
186 rocks of the Gneiss–Migmatite Complex: from ultra-high pressures
187 (22.8–20.6 kbar) but lower temperatures (617–553 °C), to eclogite-
188 facies (15.2–18.6 kbar and 672–566 °C), with amphibolite-facies over-
189 print (6.6–8.8 kbar and 570–498 °C).

190 The investigated chromitite samples were collected from small
191 chromitite pods and layers, with lengths of a few tens of meters and
192 thicknesses between <0.5 m and 2 m, except in Golyamo Kamenyane
193 where chromitite bodies are a few hundred meters long and tens of
194 meters thick. Samples of massive, semi-massive and disseminated
195 chromitites were collected from chromitite bodies of variable size
196 (Table 2).

197 Gerville et al. (2012) showed that in the Golyamo Kamenyane
198 chromitites, the metamorphism has produced four microstructural
199 types of chromites (Table 2; Fig. 2a–f): (1) partly altered chromite
200 with primary cores surrounded by porous chromite rims; (2) porous
201 chromite in which abundant pores are filled by chlorite; (3) zoned chromite
202 in which coarse grains have primary cores, sharply separated from
203 a non-porous chromite rim; (4) non-porous chromite, which hosts
204 some inclusions of chlorite and minor antigorite, and shows a polygonal
205 mosaic microstructure.

206 We re-examined the Golyamo Kamenyane chromitites and ob-
207 served that the partly altered chromites dominate the central parts of
208 the chromitite pods, whereas porous chromite is mainly found at the
209 edges or highly fractured areas. Zoned chromite and non-porous chromite
210 were only found along shears and fault zones cutting the chromitite bodies. Partly altered chromite is also preserved in the

211 small chromitite bodies in the massifs of Yakovitsa and Chernichevo,
212 whereas zoned chromite is found in sheared disseminated chromitites
213 from Yakovitsa and Avren massifs (Table 2; Fig. 2a–f). The chromite
214 grains are predominantly subhedral and less frequently anhedral with
215 a characteristic rounded shape. Individual grains may have a fracture
216 network of variable density; in the massive chromitites of Golyamo
217 Kamenyane this network was produced by shearing along faults cutting
218 the chromitite bodies. In the chromitite bodies of Chernichevo these
219 fractures are often filled with magnetite.

3. Analytical techniques

221 Selected chromite grains preserving the metamorphic patterns
222 described above were imaged using a scanning electron micro-
223 scope (SEM) model JEOL SM 6400 SEM at University of Zaragoza,
224 Spain.

225 Major (Mg, Al, Cr, Fe, Si) and minor (Ti, V, Mn, Zn and Ni) ele-
226 ments in chromite were analyzed using a CAMECA SX-50 electron
227 microprobe at Serveis Científico Técnicos of University of Barcelona,
228 Spain. The analytical conditions were 20 kV accelerating voltage,
229 20 nA beam current, and beam diameter of 3 µm. Counting times
230 were 20 s on TAP/PET and 30 s on LiF crystals. ZAF corrections were
231 applied online. The following spectral lines were monitored: Mg
232 K α , Al K α , Si K α with the TAP diffracting crystal, Ti K α and Cr K α
233 with the PET diffracting crystal, and V K α , Mn K α , Fe K α , Ni K α and
234 Zn K α with the LiF diffracting crystal. Calibration standards were
235 natural and synthetic materials: periclase (Mg), Al₂O₃ (Al), Cr₂O₃
236 (Cr), Fe₂O₃ (Fe), diopside (Si), rutile (Ti), pure V, rhodonite (Mn),
237 NiO (Ni), and sphalerite (Zn). Structural formulae of Cr-spinel were
238 calculated assuming stoichiometry, following the procedure of
239 Droop (1987). Compositions of major elements in the analyzed chro-
240 mites are listed in Supplementary Appendix A.

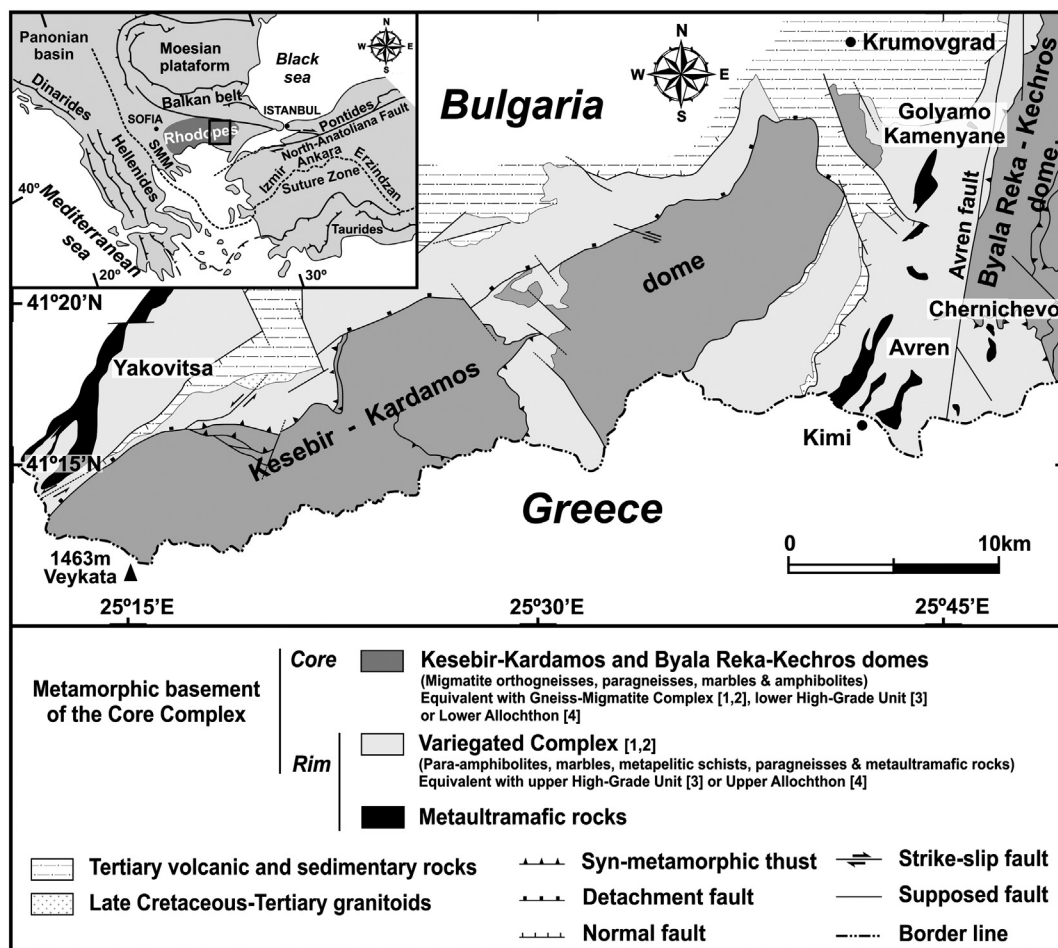


Fig. 1. Simplified geological map of the Eastern Rhodope (modified from Bonev, 2006) showing the localization of the ultramafic massifs hosting the chromitite bodies investigated in this work. Equivalence keys: 1 (Kozhoukharov et al., 1988), 2 (Haydoutov et al., 2001), 3 (Bonev, 2006), and 4 (Janák et al., 2011). Legends are in all cases inset in the figures.

242 The minor- (detected by EMPA) and trace- (detected only by LA-ICP-
 243 MS) element compositions of chromite were determined using a New
 244 Wave UP 266 laser system connected to an Agilent 7500cs ICP-MS in
 245 the Geochemical Analysis Unit, CCFS/GEMOC, Macquarie University,
 246 Sydney. For this study, the chromite analysis focused on the following
 247 masses: ^{45}Sc , ^{47}Ti , ^{51}V , ^{55}Mn , ^{59}Co , ^{60}Ni , ^{66}Zn , and ^{71}Ga . The isotopes
 248 ^{29}Si and ^{42}Ca were monitored to check for the presence of silicate
 249 inclusions.

250 The analyses were conducted using a $\sim 30\text{--}55\text{ }\mu\text{m}$ beam diameter,
 251 5 Hz frequency, and $0.032\text{--}0.105\text{ mJ/pulse}$ power, during 180 s analysis
 252 (60 s for the gas blank and 120 s on the chromite). A setup with small
 253 beam diameter ($\sim 30\text{ }\mu\text{m}$) and high power density ($3.41\text{--}7.65\text{ J/cm}^2$)
 254 was used during the measurement of the small zones free of silicates
 255 in porous chromite and thin rims of zoned and partly altered chromite.

256 The data obtained during ablation runs were processed using the
 257 GLITTER software (Griffin et al., 2009). The instrument was calibrated
 258 against the NIST 610 silicate glass (National Institute Standards and
 259 Technology, Gaithersburg, USA) (Norman et al., 1996). Aluminum
 260 values obtained by electron microprobe were used as the internal stan-
 261 dard. The basaltic glass BCR-2g (Norman et al., 1996; Gao et al., 2002)
 262 and the in-house secondary standard chromite LCR-1 (Lace mine,
 263 South Africa; Locmelis et al., 2011) were analyzed as unknowns during
 264 each analytical run to check the accuracy and precision of the analyses.
 265 The results obtained during the analyses of these two standards dis-
 266 play very good reproducibility (3%–8%) for most trace elements
 267 (Supplementary Appendix B). All laser ablation data including element
 268 concentration, 1-sigma errors and detection limits are presented in
 269 Supplementary Appendix C.

4. Results

4.1. Major elements

270 Our new electron microprobe data (Table 2 and Supplementary Ap-
 271 pendix A) for the chromites of Golyamo Kamenyane are consistent with
 272 the results of Gerville et al. (2012), showing that the partly altered
 273 chromite of semi-massive chromitites contains apparently unaltered
 274 high-Al cores with Cr# [$\text{Cr}/(\text{Cr} + \text{Al})$ atomic ratio] = 0.52–0.60, Mg#
 275 [$\text{Mg}/(\text{Mg} + \text{Fe}^{2+})$ atomic ratio] = 0.59–0.71 and $\text{Fe}^{3+}/(\text{Fe}^{3+} + \text{Fe}^{2+})$ = 0–0.30 (Figs. 3a–b and 4a). These cores are
 276 surrounded by irregular rims of porous chromite with higher values
 277 of Cr# (0.57–0.91), lower Mg# (0.44–0.68) and almost identical
 278 $\text{Fe}^{3+}/(\text{Fe}^{3+} + \text{Fe}^{2+})$ (0–0.28) (Figs. 3a–b and 4a). Grains of porous
 279 chromite have lower Mg# (0.35–0.48) but higher Cr_2O_3 (Cr# = 0.91–
 280 0.96) and $\text{Fe}^{3+}/(\text{Fe}^{3+} + \text{Fe}^{2+})$ (0.21–0.53) (Figs. 3a–b and 4a). Non-
 281 porous chromite shows Cr# = 0.96–0.99, Mg# = 0.16–0.32 and
 282 $\text{Fe}^{3+}/(\text{Fe}^{3+} + \text{Fe}^{2+})$ = 0.55–0.66 (Figs. 3a–b and 4a). Zoned chromites
 283 have cores with Cr# = 0.62–0.69, Mg# = 0.49–0.57 and $\text{Fe}^{3+}/(\text{Fe}^{3+} + \text{Fe}^{2+})$ = 0.10–0.34, surrounded by non-porous rims with
 284 lower Al_2O_3 (Cr# = 0.83–0.99) and Mg# (0.20–0.36) and higher
 285 $\text{Fe}^{3+}/(\text{Fe}^{3+} + \text{Fe}^{2+})$ (0.49–0.63) (Figs. 3a–b and 4a).

286 Like the chromitites of Golyamo Kamenyane, the other metamor-
 287 phosed chromitites of the Rhodope show an overall trend of decreasing
 288 Al_2O_3 and MgO and increasing $\text{Fe}^{3+}/(\text{Fe}^{3+} + \text{Fe}^{2+})$ from partly altered
 289 chromite to porous and non-porous chromite (Figs. 3a–h and 4a–d). In
 290 the semi-massive samples from the small body of Chernichevo, in
 291 which only partly altered chromite is preserved (Table 2), the high-Al
 292

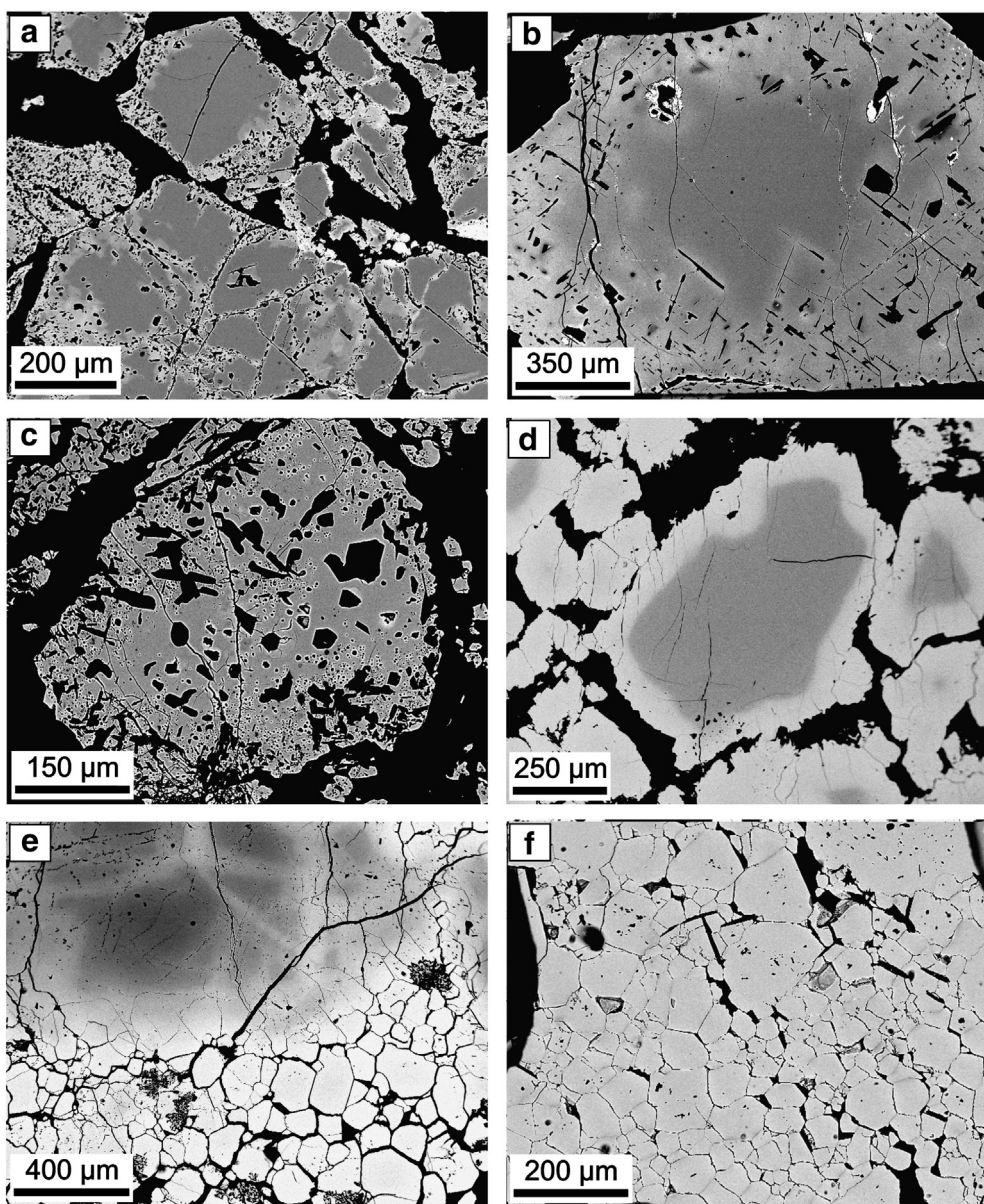


Fig. 2. Back scattered electron images of the different microstructural types of chromite that metamorphism has produced in the studied Rhodopean chromitites. Partly altered chromite with (a) thin porous rims from Golyamo Kamenyane and with (b) thick porous rims from Yakovitsa, (c) porous chromite from Golyamo Kamenyane, zoned chromite from Yakovitsa (d) and from Avren (e), and (f) non-porous chromite from Golyamo Kamenyane.

cores ($\text{Cr}\# = 0.55$, $\text{Mg}\# = 0.59$) show rims of porous chromite with higher $\text{Cr}\#$ (0.58–0.65) and lower $\text{Mg}\#$ (0.51–0.57), while $\text{Fe}^{3+}/(\text{Fe}^{3+} + \text{Fe}^{2+})$ (0.27–0.32) remains almost constant (Table 2, Figs. 3c–d and 4b).

In Yakovitsa the high-Cr cores of partly altered chromites from massive and semi-massive chromitites show higher $\text{Cr}\#$ (0.71–0.78) and $\text{Mg}\#$ (0.59–0.69) than those of disseminated chromitites ($\text{Cr}\# = 0.60$ –0.83, $\text{Mg}\# = 0.40$ –0.65) in smaller bodies (Table 2, Figs. 3e–f and 4c). Cores of grains in samples from massive and semi-massive chromitites are surrounded by rims of porous chromite with similar $\text{Cr}\#$ (0.78–0.97), but higher $\text{Mg}\#$ (0.45–0.66) and lower $\text{Fe}^{3+}/(\text{Fe}^{3+} + \text{Fe}^{2+})$ (0.18–0.43) than rims of porous chromite in disseminated chromitites ($\text{Cr}\# = 0.78$ –0.98, $\text{Mg}\# = 0.29$ –0.46, $\text{Fe}^{3+}/(\text{Fe}^{3+} + \text{Fe}^{2+}) = 0.31$ –0.50) from smaller bodies (Table 2, Figs. 3e–f and 4c). Zoned chromites preserved in disseminated samples from the smallest chromitite body (<20 cm thickness) have cores with similar $\text{Cr}\#$ (0.68–0.73) but lower $\text{Mg}\#$ (0.38–0.42)

and $\text{Fe}^{3+}/(\text{Fe}^{3+} + \text{Fe}^{2+})$ (0.08–0.17) than the cores of partly altered chromite. These cores are surrounded by rims of non-porous chromite with the highest observed $\text{Cr}\#$ (0.91–0.98) and $\text{Fe}^{3+}/(\text{Fe}^{3+} + \text{Fe}^{2+})$ (0.46–0.61), and the lowest $\text{Mg}\#$ (0.16–0.27) (Table 2, Figs. 3e–f and 4c).

Zoned chromites in the chromitites from Avren have high-Cr cores with variable $\text{Cr}\#$ (0.84–0.93) and $\text{Mg}\#$ (0.35–0.46), but weakly variable $\text{Fe}^{3+}/(\text{Fe}^{3+} + \text{Fe}^{2+})$ (0.19–0.31); these are surrounded by rims of non-porous chromite with higher $\text{Cr}\#$ (0.93–0.98) and $\text{Fe}^{3+}/(\text{Fe}^{3+} + \text{Fe}^{2+})$ (0.50–0.67), and lower $\text{Mg}\#$ (0.08–0.35) (Table 2, Figs. 3g–h and 4d).

4.1.1. Minor and trace elements

Minor- and trace-element compositions of the chromitites are presented in Supplementary Appendix C. Fig. 5 shows spidergrams with the compositions of analyzed chromites normalized to the composition of chromite from MORB plotted following the order of elements

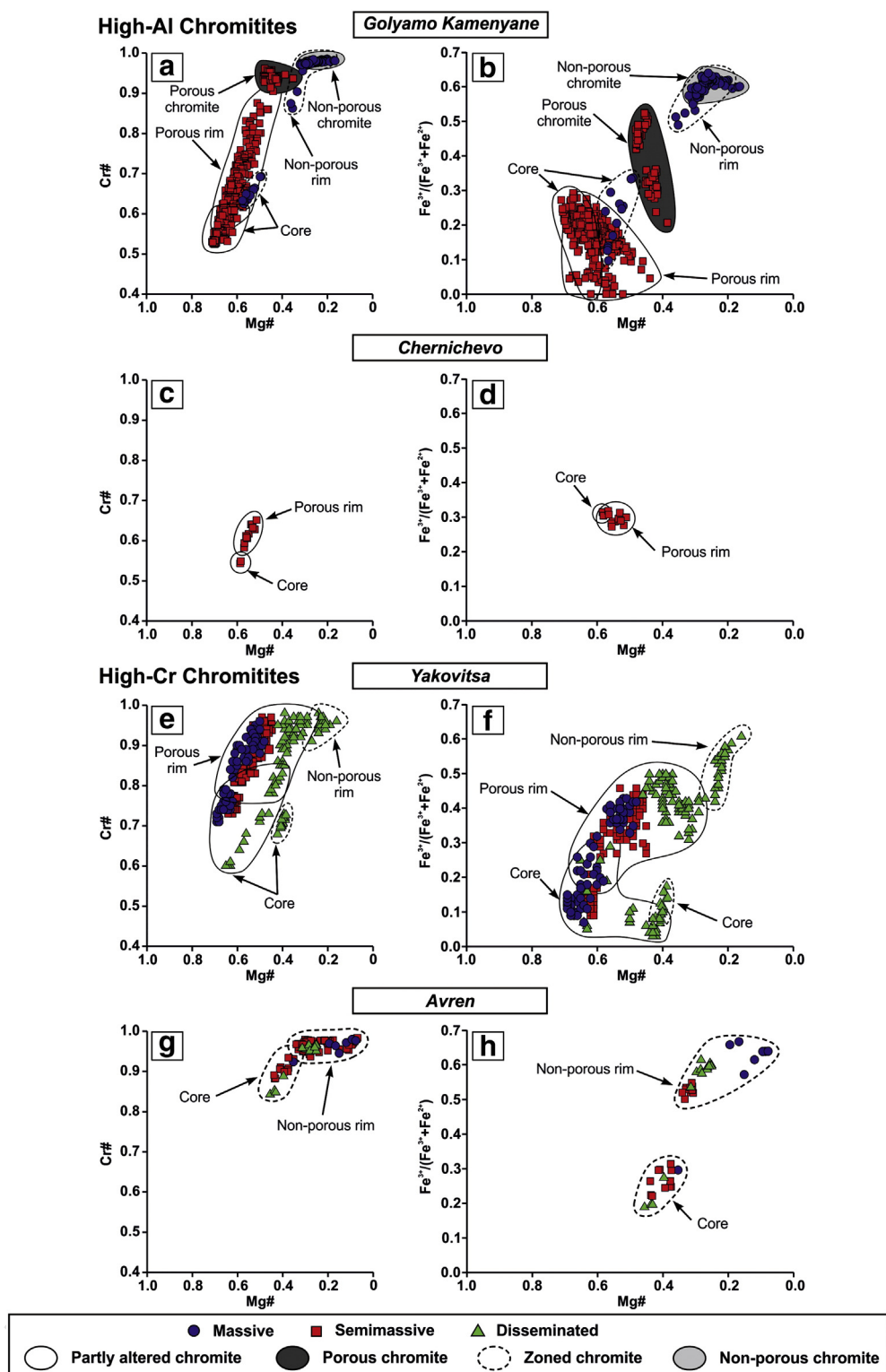


Fig. 3. Compositional variations of chromites from the studied chromitites in terms of Mg# [$\text{Mg}/(\text{Mg} + \text{Fe}^{2+})$ atomic ratio] versus Cr# [$\text{Cr}/(\text{Cr} + \text{Al})$ atomic ratio] and $\text{Fe}^{3+}/(\text{Fe}^{3+} + \text{Fe}^{2+})$. Legend is inset in the figure.

suggested by Pagé and Barnes (2009). We use the composition of this chromite as a basis for normalization because repeated laser ablation analyses show that it has a homogenous and uniform distribution of minor and trace elements.

Partly altered chromites in the semi-massive chromitites from Golyamo Kamenyane have cores and porous rims characterized by “flat” patterns with strong negative anomalies in Ti and Sc relative to

MORB (Fig. 5a–b). In contrast, grains of porous chromite with lower Al_2O_3 and MgO are more depleted in Ga, Ni, V and Sc, but slightly enriched in Ti, Zn, Co and Mn relative to the cores and porous rims of partly altered chromite (Fig. 5c). In some grains of porous chromite there is a strong M-shaped positive anomaly in the segment Zn–Co–Mn (hereafter ZCM-anomaly; Fig. 5c). Grains of porous chromite have cores with lower contents of Ti, Zn, Co and Mn than

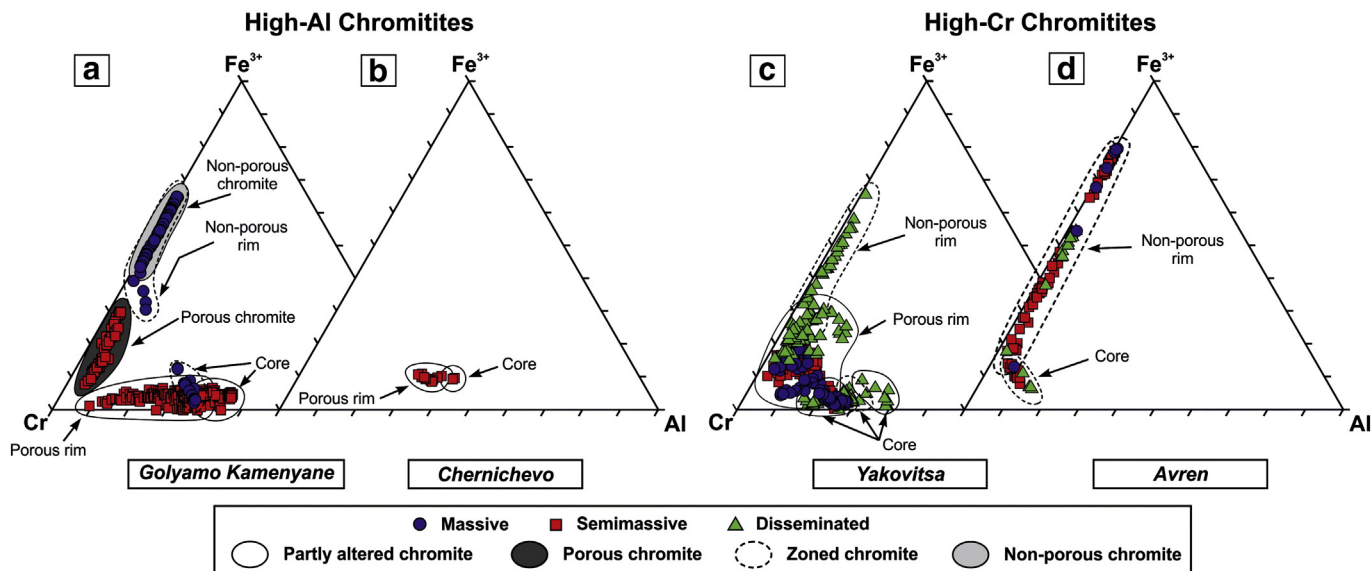


Fig. 4. Variations of Al^{3+} , Cr^{3+} and Fe^{3+} in chromites from the studied chromitites. Legend is inset in the figure.

their outermost parts, but with higher contents of V and similar contents of Ga, Ni, and Sc. The cores of zoned chromite grains in massive chromitites also show strong depletion in Sc, Ni, Ga and Ti, while the enrichment in the segment $\text{Zn}-\text{Co}-\text{Mn}$ does not define a ZCM-anomaly (Fig. 5d). The latter pattern is distinctly different from that of non-

porous chromite (also found surrounding these cores) which has lower Al_2O_3 but higher Ga, Ti, Ni and Sc, and the ZCM-anomaly (Fig. 5e-f).

Partly altered chromites from Chernichevo have cores and rims showing almost identical flat trace-element patterns. Relative to MORB chromite, the chromitites from Chernichevo show a distinct

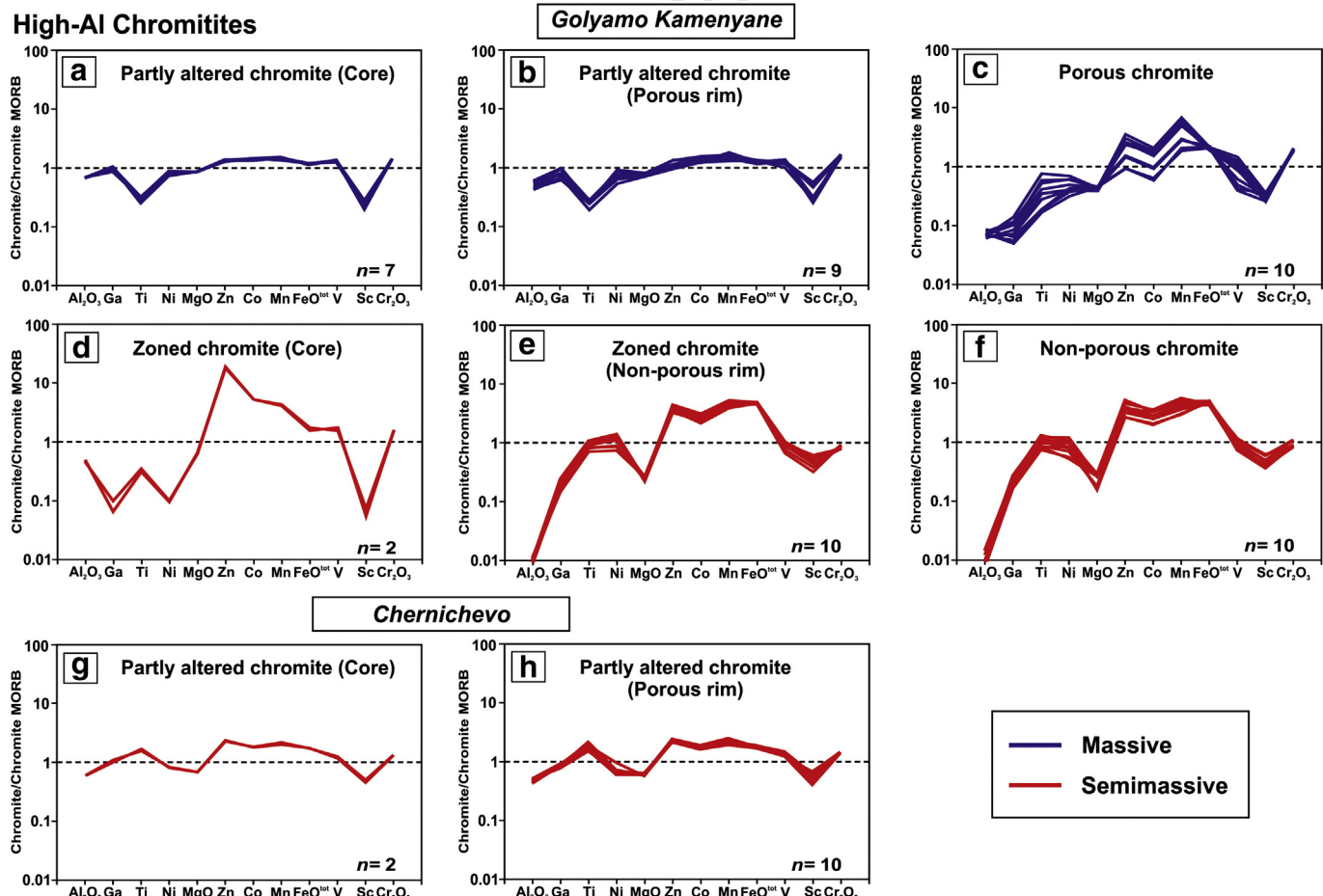


Fig. 5. Spidergrams showing the composition (major, minor and trace elements) of the different microstructural types of chromite from the studied Rhodopean chromitites. The analyzed compositions are normalized to the composition of chromite from MORB (Pagé and Barnes, 2009). Legend is inset in the figure.

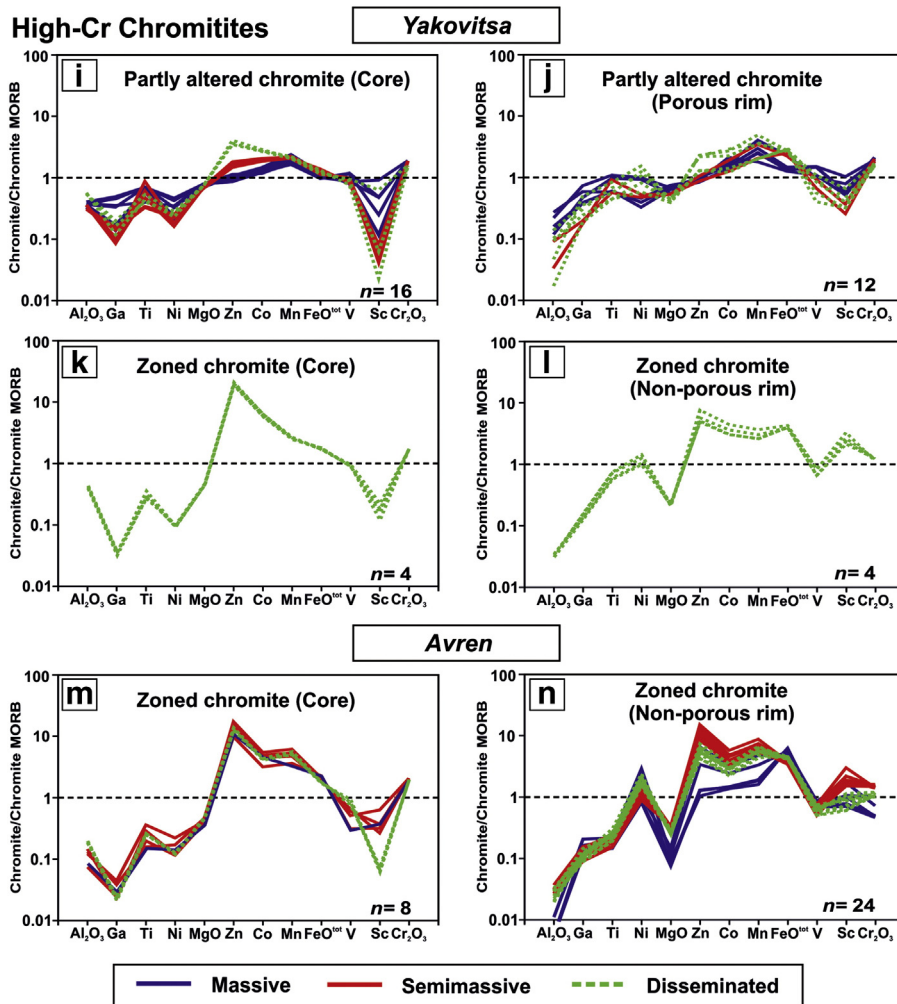


Fig. 5 (continued).

enrichment in Ti coupled with a less marked ZCM-anomaly and depletion in Sc (Fig. 5g–h).

In the Yakovitsa occurrence, the high-Cr cores of partly altered chromites show positive slopes in their patterns, produced by depletion in Ga, Ti, Ni and Sc, and enrichment in Zn, Co and Mn relative to MORB chromite (Fig. 5i). The first segment of the pattern is characterized by enrichment in Ti relative to Ga and Ni. The cores of partly altered chromite from the massive chromitites have higher contents of Ga, Ti, Ni and Sc and lower Zn and Co than the cores of chromites from smaller bodies of disseminated chromitite (Fig. 5i). The rims of porous chromite surrounding these cores show substantially different patterns, with slightly higher contents of Ga, Ni, Mn and Sc but overall lower Al₂O₃ and V (Fig. 5j). Zoned chromites in the disseminated chromitites have cores with patterns almost identical to the cores of zoned chromites of the Golyamo Kamenyane chromitites (Fig. 5d and k). These cores are depleted in Ga, Ti, Ni and Sc, and enriched in Zn, Co and Mn relative to chromite from MORB, but are enriched in Ti relative to Ga and Ni and show a pronounced positive anomaly in Zn (Fig. 5k). However, the rims surrounding these cores have much higher contents of Sc (producing a positive anomaly) as well as Ga, Ti and Ni, but lower Zn, Co and Mn (Fig. 5l).

The zoned chromites of Avren show high-Cr cores with trace-element patterns somewhat similar to that of the cores of zoned chromites from Golyamo Kamenyane and Yakovitsa (Fig. 5d, k and m). In contrast, the rims of non-porous chromite show a gentler slope in the

segment Ga–Ti, coupled with a marked positive anomaly in Ni and a negative one in MgO (Fig. 5n). These patterns also show the typical ZCM-anomaly and enrichment in Sc relative to MORB chromite, like the similar rims from Yakovitsa (Fig. 5l and n).

5. Discussion

5.1. Metamorphism of the chromitites of the Eastern Rhodopes

Gervilla et al. (2012) explained the origin of the different microstructures of chromitites in the Golyamo Kamenyane massif as the consequence of a two-stage process involving the infiltration of fluids during the retrograde metamorphic evolution of the Rhodope Metamorphic Core Complex.

During the first stage, the hydration of olivine from the host dunite released significant amounts of H₂, which contributed to a much lower fO₂ by its reaction with O₂ to form water (e.g., Bach et al., 2006). In the chromitite bodies, the infiltration of these reducing fluids probably promoted the reaction of primary chromite with matrix olivine, giving rise to chlorite and to secondary chromite residually enriched in Cr and Fe²⁺ by loss of Al₂O₃ and MgO to the chlorite (Fig. 6). This metamorphic event is well recorded in the partly altered chromites of Golyamo Kamenyane, which show a decrease in Mg# (0.59–0.71), and an increase in Cr# (0.52–0.60), but nearly unchanged Fe³⁺/(Fe³⁺ + Fe²⁺) (0–0.30), from core to rim (Mg# = 0.44–0.68,

400 Cr# = 0.57–0.91 in the porous rim; Fig. 3a–b). This replacement involves mass loss from chromite grains without changes in their size, 401 resulting in the formation of pores (i.e. porous chromite), which may 402 be filled by the chlorite produced during the reaction (Figs. 2a–c and 403 6). Thermodynamic modeling by Gerville et al. (2012) suggests that 404 this reaction took place during cooling of the rocks through an interval 405 from ~700 to ~450 °C.

406 Once olivine was exhausted in the host dunite and the chromitite, the 407 fO_2 shifted progressively to higher values (i.e., more oxidizing conditions; 408 Alt and Shanks, 1998; Allen and Seyfried, 2003; Bach et al., 2004; 409 Alt et al., 2007). This variation in fO_2 changed the conditions of chromite 410 alteration, producing a different type of metamorphic chromite. These 411 fluids with progressively higher fO_2 infiltrated the network of pores in 412 the Cr- and Fe^{2+} -rich porous chromite, depositing magnetite while 413 dissolving chlorite in the pores, thus promoting the diffusion of Fe^{2+} 414 and Fe^{3+} into chromite and eliminating the porous textures to produce 415 a non-porous chromite significantly enriched in Fe^{3+} (i.e. ferrian 416 chromite; Fig. 6). Fe^{2+} and Fe^{3+} can easily diffuse through the porous 417 rims of the chromite grains but diffusion is slower in the unaltered, 418 non-porous core, which results in the formation of zoned 419 chromite (Fig. 2d–e). This explains why in the zoned chromites of 420 Golyamo Kamenyane there is an increase in $Fe^{3+}/(Fe^{3+} + Fe^{2+})$ 421 (0.10–0.34) and Cr# (0.62–0.69), and a decrease in Mg# (0.49–0.57), 422 from core to rim ($Fe^{3+}/(Fe^{3+} + Fe^{2+}) = 0.49–0.63$, Cr# = 0.83– 423 0.99, Mg# = 0.20–0.36, in the non-porous rim; Fig. 3a–b). During this 424 second stage, which might also involve the transformation of some 425 chlorite to antigorite, the amount of Fe^{2+} and Fe^{3+} supplied by the 426 infiltrating fluids might exceed the volume of pre-existing pores, promoting 427 the coarsening of chromite to produce non-porous chromite with 428 mosaic or polygonal textures (Figs. 2f and 6).

429 Phase relations in the system $(Fe^{2+}, Mg)Cr_2O_4$ – (Fe^{2+}, Mg) 430 $Fe^{3+}_2O_4$ – $(Mg)Al_2O_4$ suggest that the studied non-porous chromite 431 could form at temperatures near 600 °C (Sack and Ghiorso, 1991; 432 Gerville et al., 2012), overlapping the formation of Fe^{2+} -rich chromite. 433 According to Gerville et al. (2012), in the Golyamo Kamenyane Massif 434 both stages in the alteration of chromite took place as the rocks cooled 435 from ~700 to ~450 °C along the eclogite- to amphibolite-facies retro- 436 grade metamorphic pathway (Mposkos and Krohe, 2000, 2006; 437 Mposkos, 2002; Haydoutov et al., 2004) associated with the exhumation 438 of the allochthonous rim of the eastern Rhodope. 439

440 The microstructures and chemical variations of chromite from the 441 other metamorphosed chromitites of the Eastern Rhodope can also be 442 interpreted in terms of the two-stage process described for the chromites 443 of Golyamo Kamenyane (Gerville et al., 2012) (Fig. 6). Evidence 444 for the first stage is preserved as Cr- and Fe^{2+} -rich porous rims sur- 445 rounding the cores of partly altered chromite in the Chernichevo 446 (high-Al chromites) and Yakovitsa (high-Cr chromites). In the latter 447 the reaction of high-Cr chromite with the olivine matrix had produced 448 Cr-rich clinochlore, similar to that replacing high-Cr chromites in the 449 nearby Dobromirtschi Ultramafic Massif (González Jiménez et al., 2009) 449 and metamorphosed chromitites elsewhere (e.g., Jan and Windley, 450 1990; Merlini et al., 2009; Mukherjee et al., 2010). In chromitites from 451 Chernichevo and Yakovitsa, the oxidizing second stage did not 452 completely erase the pores, but only contributed to increase the magne- 453 tite component in the Fe^{2+} -rich porous chromite (Table 2; Figs. 3c–f 454 and 6). In contrast, in some of the disseminated chromitites in the 455 smallest chromitite bodies in Yakovitsa and Avren, the oxidizing fluids 456 were able to precipitate enough material in the cavities of porous chro- 457 mite to produce zoned and non-porous chromite (Table 2; Figs. 3e–h 458 and 6).

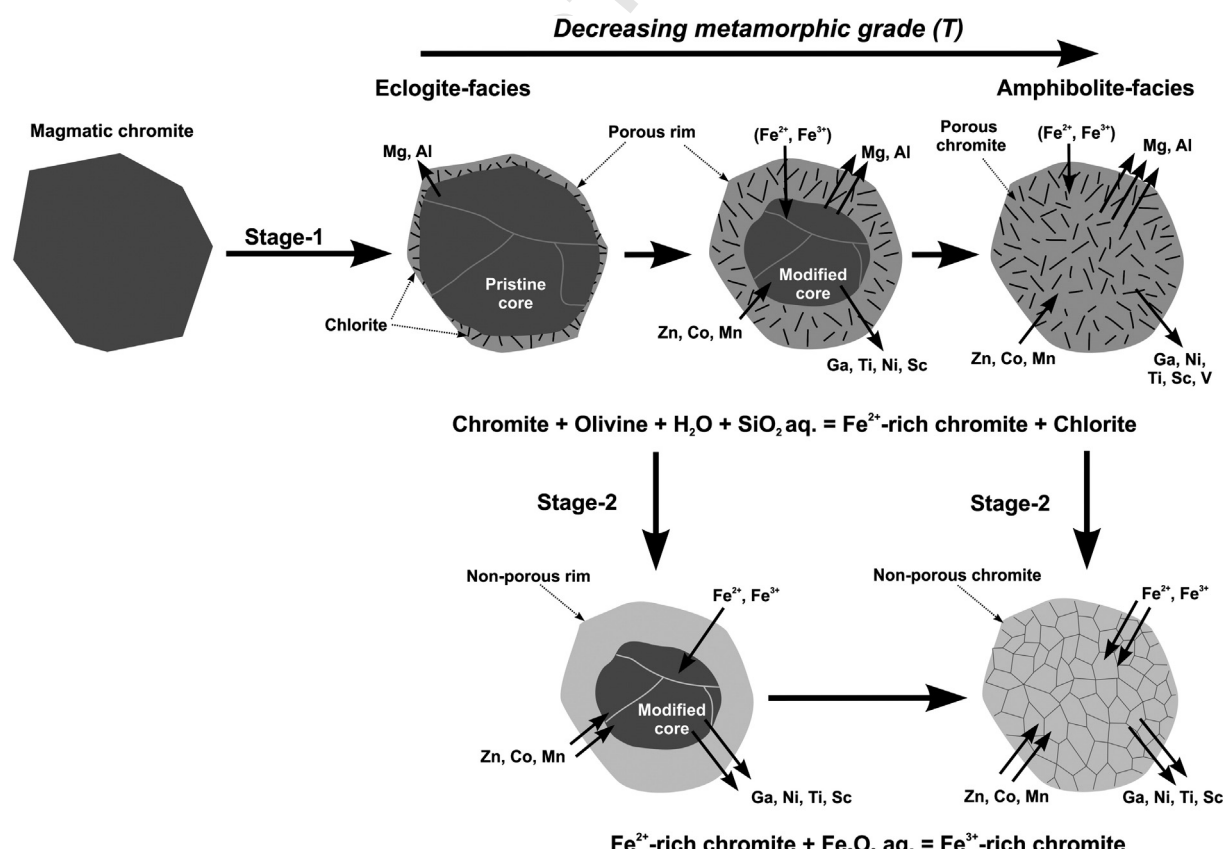


Fig. 6. Schematic illustration of microstructural and chemical (major, minor and trace elements) changes in chromites, showed as two-stage processes of alteration during the retrograde evolution of chromitites from the eastern Rhodopes. The extent of reaction is noted in the figure with number of arrows.

The preservation of porous chromite rims and/or their obliteration by the formation of rims of non-porous chromite is directly associated with the ability of the infiltrating fluids to penetrate the chromite. The effectiveness of the altering fluids would depend on (1) their ability to penetrate chromite, mainly controlled by the chromite/silicate ratio and the presence of secondary permeability such as fractures; (2) the availability of enough fluid to allow higher rates of interaction between the infiltrating fluids and chromite. The fact that some grains only show porous textures whereas others have compositionally-distinct porous rims of variable thickness (Fig. 2a–c; Table 2) shows that the alteration process did not operate in the same way in different parts of individual chromitite bodies. Zoned and non-porous chromites are mostly found in sheared chromitites collected from faults cutting the bodies. This clearly indicates that a strong fracture network and associated deformation facilitated the circulation of fluids, helping the nucleation and/or dynamic recrystallization of ferrian chromite (Satsukawa et al., 2014).

Gervilla et al. (2012) noted that in the Golyamo Kamenyane massif chromitites are cut by veins of anthophyllite, whereas veins filled by asbestos and talc cut chromitites in the Avren massif. In this scenario, shear zones probably acted as channels for focused migration of the oxidizing fluids producing the nearly complete replacement of the pre-existing porous chromite by Fe^{3+} -rich non-porous chromite. This focused infiltration of the oxidizing fluids along the shear zones would prevent the obliteration of the porous textures in the rest of the massif (e.g., areas outside the shear zones). An almost complete replacement of porous chromite by non-porous chromite in these shear zones can explain why we do not observe grains with inner rims of porous chromite and outer rims of non-porous chromite in some of the chromitites from Golyamo Kamenyane, Yakovitsa and Avren (Fig. 2). This is consistent with the observations that veins of anthophyllite cut some chromitites in Golyamo Kamenyane (Gervilla et al., 2012) and veins of asbestos and talc cut some at Avren (Kolkovski et al., 2003).

5.2. Trace-element fingerprints of metamorphism in the cores of partly altered chromites

The high-Cr cores of partly altered chromite in massive and semi-massive chromitite bodies (>40 cm thickness) from Yakovitsa have higher Mg# (0.59–0.69) than chromite in thinner bodies (20–30 cm thickness) made up only of disseminated chromitite (Mg# = 0.40–0.65) (Table 2; Fig. 3e–f). This trend of enrichment of Fe^{2+} (i.e., higher contents in cores of chromite from disseminated samples relative to those from massive chromitites) is somewhat similar to that described in grains of chromite from unmetamorphosed massive and disseminated chromitites in ophiolites elsewhere (e.g., Leblanc and Nicolas, 1992). It is usually attributed to the diffusion of Fe^{2+} and Mg^{2+} between chromite and olivine at high temperatures (1000–900 °C) during post-magmatic cooling (Table 1; Barnes, 2000; Kamennetsky et al., 2001; Rollinson et al., 2002). However, Candia and Gaspar (1997) have reported similar trends in chromite grains that have re-equilibrated with the host olivine matrix during metamorphism at 750–700 °C and $P_{H_2O} = P_{tot}$. These conditions are similar to those of the eclogite-facies metamorphism that affected the chromitites of the Eastern Rhodope (775–750 °C; Mposkos and Krohe, 2000, 2006; Mposkos, 2002; Gervilla et al., 2012). The microstructures and the variations of Mg#, Cr# and $Fe^{3+}/(Fe^{3+} + Fe^{2+})$ in the cores of partly altered chromites from Yakovitsa do not allow discrimination between the two processes.

To further assess the effects of metamorphism on the cores of partly altered chromites from Yakovitsa we have compared their minor- and trace-elements patterns with the composition of high-Cr chromites from an unmetamorphosed chromite body of similar size. The chromitite dike selected is from the locality of Dyne in the New Caledonia Ophiolite and has cross-section dimensions of 8.5×0.5 m (Leblanc et al., 1980; Cassard et al., 1981; Fig. 7a–b). The chromite grains from Dyne have experienced extensive sub-solidus $Mg^{2+} \leftrightarrow Fe^{2+}$ exchange with olivine

during cooling; it is recorded by the decrease of Mg# at constant Cr# in the chromites with lower chromite/silicate ratios (Fig. 7b). The patterns of minor- and trace elements in the unmetamorphosed chromite grains of Dyne are almost identical to those of high-Cr chromite in massive chromitites from unmetamorphosed ophiolites (Fig. 7a) such as Thetford Mines (Pagé and Barnes, 2009) and Eastern Cuba (González-Jiménez et al., 2013, 2014), which make them very useful to our propose.

The cores of partly altered chromites from Yakovitsa have patterns distinctly different from the “unmetamorphosed” chromites of Dyne, being more depleted in Ga and Sc, and enriched in Zn, Co and Mn; the concentrations of Ti can be higher or lower (Fig. 5i and 7a). Despite these notable differences, both the unmetamorphosed chromites from Dyne and the cores of partly altered chromites from Yakovitsa show a similar negative correlation between Ga and $Zn + Co + Mn$ as Mg# decreases at lower chromite/silicate ratio (Fig. 7b–c). However, in the unmetamorphosed chromites of Dyne the decrease of Mg# occurs at constant Cr#, whereas the decrease of Mg# in the cores of partly altered chromites from Yakovitsa is associated with an increase of Cr#, driven by the formation of porous rims and the sequestering of Al and Mg into the metamorphic chlorite. Gallium, like Al, is a trivalent cation that does not enter the olivine lattice but can be taken up by chlorite (up to 31 ppm in our samples; Table 1). This suggests that the negative correlation of Ga vs $Zn + Co + Mn$ observed in Fig. 7c could be a consequence of the metamorphism rather than of subsolidus re-equilibration between chromite and olivine during cooling.

Gallium, Ni, Sc and Ti decrease from the inner to the outer part in the cores of partly altered chromite at a relatively constant Mg# (Fig. 8a–d), but these have complex relationship to $Fe^{3+}/(Fe^{3+} + Fe^{2+})$ (Fig. 8e–h). In the cores of partly altered chromite of massive chromitites there are no correlations among Ga, Ni, Sc, Ti and $Fe^{3+}/(Fe^{3+} + Fe^{2+})$, whereas the latter increase from the inner to the outer part in the cores of partly altered chromites of semi-massive and disseminated chromitites (Fig. 8e–h). This suggests that the diffusion of minor- and trace elements from core to Fe^{2+} -rich porous rims in partly altered chromites results from the re-ordering of Fe^{2+} and Fe^{3+} into octahedral and tetrahedral sites (Fig. 1 in Sack and Ghiors, 1991), which promoted the entrance of Ni^{2+} into octahedral positions and Ga^{3+} , Sc^{3+} and Ti^{4+} into the tetrahedral sites. The latter effect, combined with the higher degree of infiltration of fluids into chromitites with lower chromite/silicate ratios, produced thicker rims of Fe^{2+} -rich porous chromite, promoting higher mobilization and enrichment of Ga, Ni, Sc and Ti, from cores to porous rims in partly altered chromites (Figs. 5i–j and 6).

The highest values of Zn, Co and Mn, and very low Mg#, occur in cores of partly altered chromites in disseminated samples (Fig. 8i–k). This may indicate a greater degree of substitution in samples with higher proportions of olivine (González Jiménez et al., 2009). Zinc, Co and Mn, together with Fe^{2+} , can enter the tetrahedral sites vacated by Mg^{2+} sequestered into olivine during cooling and subsolidus re-equilibration between chromite and olivine, as is observed in the unmetamorphosed chromites of Dyne (Table 1; Fig. 7b). However, the coincidence of enrichment in Zn, Co and Mn with stronger depletion in Ga, Sc and Ni (Fig. 7c), and the fact that all of these elements show very distinct correlations with $Fe^{3+}/(Fe^{3+} + Fe^{2+})$ (Fig. 8l–n), suggest a complex interplay of substitutions during the metamorphism. Thus the contents of Mn increase from the inner to the outer parts of the cores in massive samples at constant $Fe^{3+}/(Fe^{3+} + Fe^{2+})$, but are constant as $Fe^{3+}/(Fe^{3+} + Fe^{2+})$ increases in semi-massive and disseminated ones (Fig. 8n). This suggests that in samples with the lowest chromite/silicate ratio, the formation of Fe^{2+} -rich porous chromite promotes the re-ordering of Fe^{2+} , limiting the substitution of Fe^{2+} (in octahedral sites) by Mn^{2+} , Zn and Co (Fig. 6). This can explain why, in these cores of partly altered chromite, Zn and Co decrease with increasing $Fe^{3+}/(Fe^{3+} + Fe^{2+})$ (Fig. 8l–m). Taken together these observations suggest that the positive ZCM-anomaly, coupled with depletion in Ga, Ni and Sc, is a fingerprint of amphibolite-facies metamorphism in the high-Cr cores of partly altered chromites from Yakovitsa. These

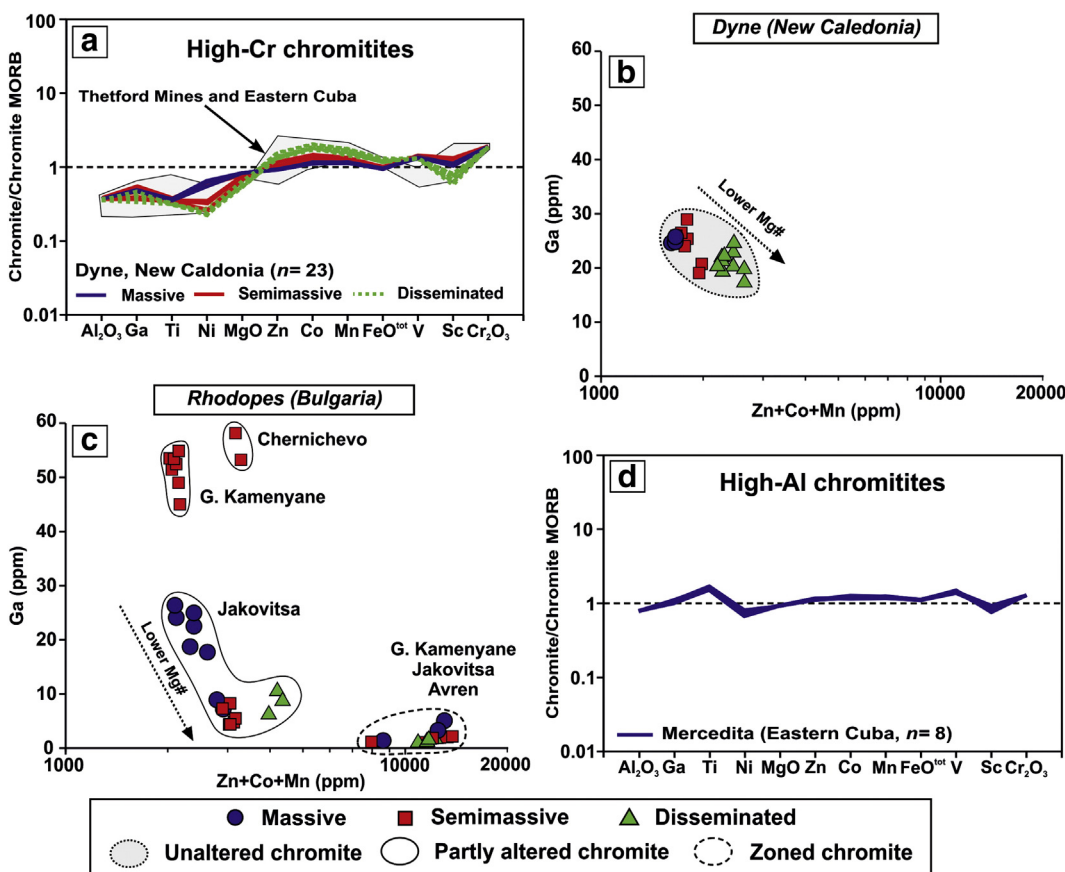


Fig. 7. Spidergrams showing the composition (major, minor and trace elements) of high-Cr chromite in unmetamorphosed massive chromitites from Thetford Mines (Pagé and Barnes, 2009) and Eastern Cuba (González-Jiménez et al., 2013, 2014), and from the chromitite dike of Dyne (New Caledonia Ophiolite) (a). Compositional variation in terms of Zn + Co + Mn (ppm) vs. Ga (ppm) of unmetamorphosed chromites from the chromitite dike of Dyne (New Caledonia Ophiolite) (b) and chromite cores from the studied Rhodopean chromitites (c). Spidergrams showing the major, minor and trace elements composition in high-Al chromite from unmetamorphosed massive chromitites of Mercedita (Eastern Cuba) (d). The analyzed compositions are normalized to the composition of MORB chromite (Pagé and Barnes, 2009). Legend is inset in the figure.

chemical variations were produced, or strengthened, by the exchange of cations between these cores and their surrounding porous rims filled with chlorite (Fig. 6).

On the other hand, the cores of partly altered high-Al chromites from Golyamo Kamenyane and Chernichevo show elemental patterns almost identical to their surrounding porous rims (Fig. 5a–b and g–h). This may suggest that either (1) the infiltrating fluids did not substantially modify the trace- and minor elements or (2) an almost complete re-equilibration was reached between the cores and their surrounding rims. The first alternative is supported by the fact that the patterns of those cores are practically identical to the “flat” patterns of high-Al massive chromitites in the unmetamorphosed ophiolites of Eastern Cuba (Fig. 7d). The porous rim of partly altered chromites from Golyamo Kamenyane and Chernichevo is very thin (Fig. 2a), indicating that a limited reaction between cores and infiltrating fluids prevented an extensive exchange of elements (Fig. 6). In contrast, higher fluid/rock ratios promoted higher rates of reaction between the small grains of chromite and infiltrating fluids, resulting in complete replacement by porous chromite in Golyamo Kamenyane (Fig. 6). This can explain why these grains exhibit the ZCM-anomaly coupled with strong depletion in Ga, Ni, Sc and V, as preserved in the modified cores of partly altered chromites from Yakovitsa (Fig. 5c and i).

In the grains of porous chromite from Golyamo Kamenyane there are also complex relationships between the trace elements and Fe^{3+} / $(\text{Fe}^{3+} + \text{Fe}^{2+})$ (Fig. 8o–v). Thus, during the reaction of primary chromite with olivine in the presence of reducing fluids, Mg^{2+} and Ni^{2+} would be lost from the chromite, while Fe^{2+} was added together with Zn, Co and Mn (Fig. 6). This Fe^{2+} -rich chromite has a normal spinel

structure but with fewer available octahedral sites than the pristine chromite (Sack and Ghiorso, 1991), thus explaining their relative depletion in Ga, V and Sc (Fig. 6). Interestingly, the grains of porous chromite exhibit a wider range of Ti and higher Fe^{3+} contents (in octahedral sites) than the porous rims of partly altered chromite grains (Fig. 8v). This suggests that the porous chromite grains had re-equilibrated to a greater extent with infiltrating fluids rich in Fe^{3+} , added during the second stage of alteration. These fluids did not contribute to eliminating the pores in the porous chromite but promoted the re-ordering of octahedral sites in the chromite lattice and thus, facilitated the incorporation of Ti^{4+} (Fig. 6).

5.3. Minor- and trace elements and the precipitation of ferrian chromite

As noted above, the second stage of alteration during the metamorphism of the Rhodopean chromitites involved the infiltration of oxidizing fluids through the pores of the porous chromite, to produce non-porous rims or grains of ferrian chromite (Gervilla et al., 2012).

The non-porous rims of ferrian chromite on the zoned chromites from the high-Cr (Yakovitsa and Avren) and high-Al chromitites (Golyamo Kamenyane) show very similar patterns of minor- and trace elements (Fig. 5e, l and n). These profiles are identical to that observed in non-porous ferrian chromite in the Golyamo Kamenyane chromitites (Fig. 5f), which suggests their alteration by a common fluid that has obliterated the geochemical fingerprint of the pre-existing chromite regardless of its original composition. Interestingly, the cores of the zoned chromites show patterns with very similar shapes, although very different to those of their surrounding rims. Overall, these cores are more

644 depleted in Ga, Ni and Sc and more enriched in Zn and Co (Fig. 5d, k and
 645 m) than the non-porous ferrian chromite. The profiles of these cores of
 646 zoned chromites are distinctly different from those of the cores of partly

647 altered chromites within the same chromitite body, indicating how 648 their composition was influenced by reaction with a specific type of 649 rim (i.e. Fe^{2+} -rich and porous vs Fe^{3+} -rich and non-porous). The 649

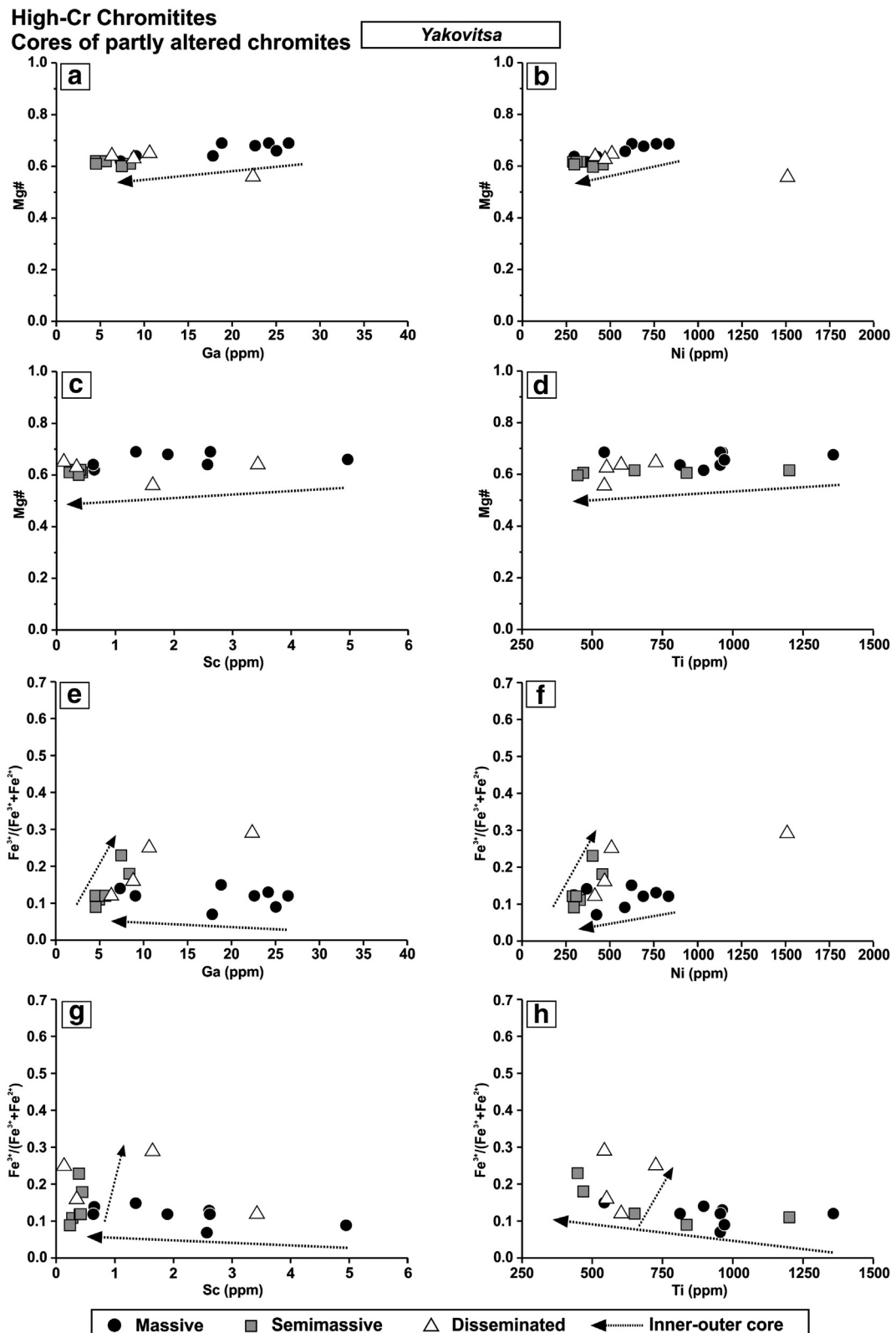


Fig. 8. Compositional variations in the high-Cr cores of partly altered chromite from Yakovitsa in terms of Zn, Co, Mn, Ga, Ni, Sc and Ti (in ppm) versus Mg# [$\text{Mg}/(\text{Mg} + \text{Fe}^{2+})$ atomic ratio] and $\text{Fe}^{3+}/(\text{Fe}^{3+} + \text{Fe}^{2+})$ (a–n). Variations of Ni, Zn, Co, Mn, Ga, V, Sc and Ti contents (in ppm) versus $\text{Fe}^{3+}/(\text{Fe}^{3+} + \text{Fe}^{2+})$ in the porous rims of partly altered chromite and the porous chromite of high-Al chromitites at Golyamo Kamenyane (o–v). Legend is inset in the figure.

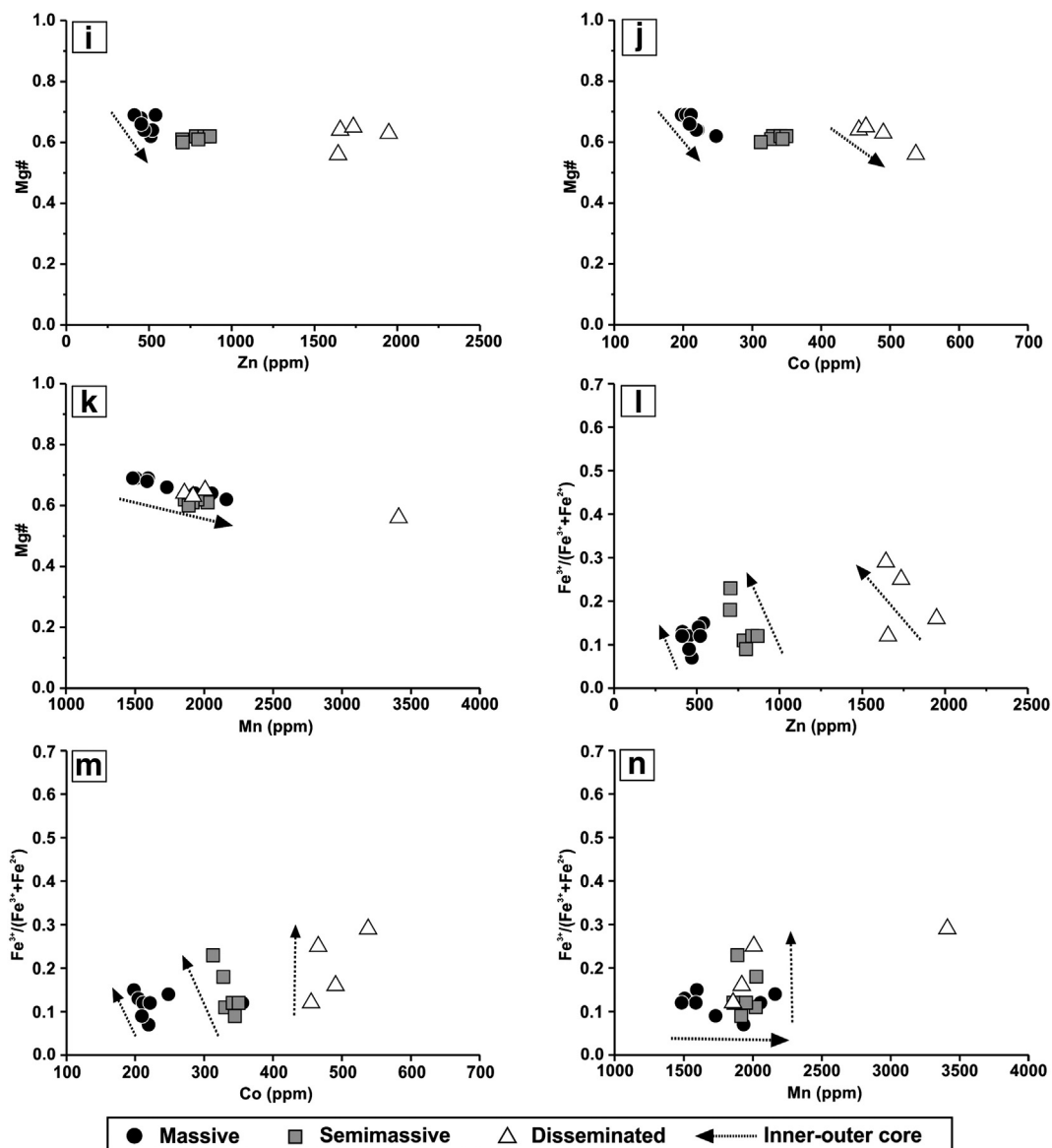


Fig. 8 (continued).

650 differences can be explained by the re-ordering of Fe²⁺ and Fe³⁺ in octahedral sites in the non-porous ferrian chromite rims, which limits the 651 uptake of Ga³⁺, Ni²⁺ and Sc³⁺ but allows the diffusion of Zn, Co (and 652 Mn) toward the cores (Fig. 6). The Ti contents in cores of the zoned 653 chromites of Yakovitsa are lower than those of the partly altered chromite, 654 suggesting that in samples from small chromitite bodies (<20 cm thick) and with lower chromite/silicate ratios, Ti⁴⁺ also dif- 655 fuses from core to rim (Fig. 6).

658 6. Conclusions

659 (1) Eclogite- to amphibolite-facies retrograde metamorphism has 660 produced four microstructural types of chromite in the 661 Rhodopean chromitites: (1) porous chromite, enriched in Cr 662 and Fe²⁺ and depleted in Al, with chlorite filling the pores; 663 (2) partly altered chromite, with primary cores surrounded by 664 porous chromite; (3) non-porous chromite, enriched in Fe³⁺ 665 (i.e. ferrian chromite) with polygonal mosaic microstructure, 666 and (4) zoned chromite, with primary cores surrounded by 667 non-porous chromite.

668 (2) High-Cr cores and porous rims surrounding them in partly al- 669 tered chromites are enriched in Zn, Co and Mn (ZCM-anomaly) 670 and depleted in Ga, Ni and Sc. This distribution of minor- and 671 trace elements is the result of the exchange (i.e., diffusion) of 672 minor- and trace elements between cores and their surrounding 673 rims (with higher contents of Ga, Ti, Ni Mn, and Sc, but lower in 674 V) concomitant with the crystallization of chlorite in the pores. 675 We propose this ZCM-anomaly as a fingerprint of amphibolite- 676 facies metamorphism.

677 (3) High-Al cores of partly altered chromites and their thin sur- 678 rounding porous rims show identical trace-element patterns, 679 which suggest a more limited reaction between these cores and 680 infiltrating reducing fluids. Such a limited exchange of elements 681 does not substantially modify the original composition in chro- 682 mite cores.

683 (4) Small grains of high-Al porous chromite are significantly more 684 enriched in Zn, Co and Mn (ZCM-anomaly) and depleted in Ga, 685 Ni, Sc and V than rims on partly altered chromite. This suggests 686 greater element mobility as a result of almost complete infiltration 687 of altering fluids.

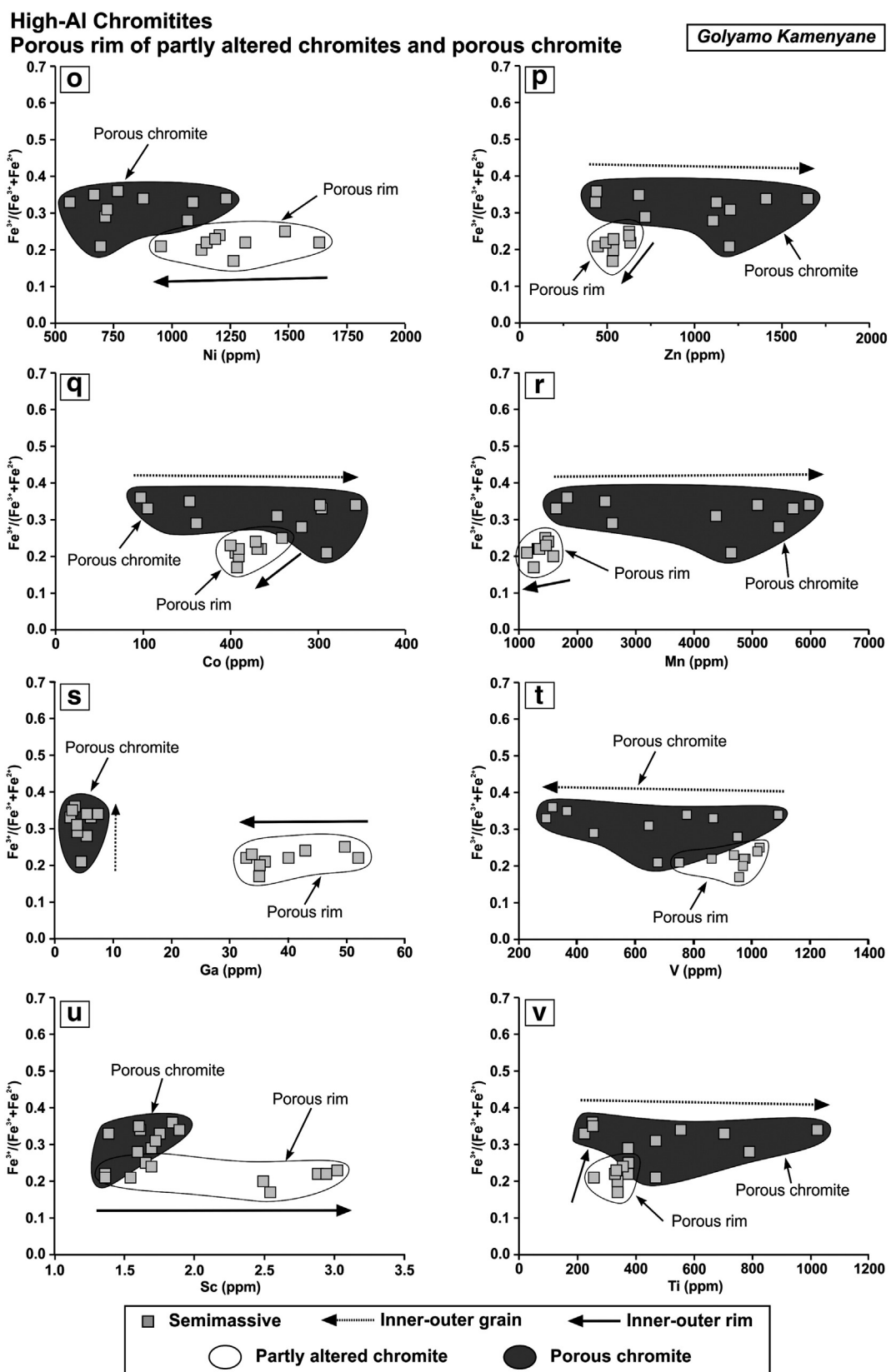


Fig. 8 (continued).

688 (5) Non-porous chromite grains and rims on cores of zoned chromite
 689 in high-Cr and high-Al chromitites exhibit similar patterns of
 690 minor- and trace elements, suggesting their equilibration with
 691 a common oxidizing fluid. This fluid, rich in the magnetite

692 component, has obliterated the geochemical signatures of the
 693 pre-existing chromite regardless of its original composition.
 694 (6) Within a single ultramafic massif, the cores of zoned chromite
 695 grains show a distinctive pattern (depleted in Ga, Ni and Sc but

enriched in Zn and Co, relative to non-porous rims) different from the cores of partly altered chromite grains. This reflects the interaction of chromite cores with rims formed by a distinct type of fluid (i.e. Fe^{2+} -rich in the porous chromite vs Fe^{3+} -rich in the non-porous chromite).

(7) This study reveals that the in-situ analysis of minor- and trace elements in chromite using LA-ICP-MS may help to recognize fingerprints of metamorphism. This is valuable information that may limit incorrect interpretations of the petrogenesis of the chromite host rocks. Additionally, the metamorphic fingerprints identified in this paper can be applied to the study of isolated chromite grains in serpentinites elsewhere. We expect that the disturbance of trace- and minor elements by metamorphism is much more effective in chromites from peridotites than in chromitites, as the former have lower chromite/silicate ratios that allow higher rates of reaction between infiltrating fluid and chromite. Very likely it would result in more complex patterns than those observed here. This suggestion can be the basis of future studies.

Supplementary data to this article can be found online at <http://dx.doi.org/10.1016/j.chemgeo.2014.10.001>.

Acknowledgments

This paper is a contribution to project CGL2010-15171 and F.P.I. grant BES-2011-045423 of the Spanish Ministry of Economy and Competitiveness. The analytical data were obtained using instrumentation funded by DEST Systemic Infrastructure Grants, ARC LIEF, NCRIS, industry partners and Macquarie University. This is a contribution XXX from the ARC National Key Centre for Geochemical Evolution and Metallogeny of Continents (<http://www.gemoc.mq.edu.au>) and paper XXX from the ARC Centre of Excellence for Core to Crust Fluid System (<http://www.ccfs.mq.edu.au>).

References

Abzalov, M.Z., 1998. Chrome-spinels in gabbro–wehrlite intrusions of the Pechenga area, Kola Peninsula, Russia: emphasis on alteration features. *Lithos* 43 (3), 109–134.

Ahmed, A.H., Arai, S., Abdel-Aziz, Y.M., Rahimi, A., 2005. Spinel composition as a petrogenetic indicator of the mantle section in the Neoproterozoic Bou Azzer ophiolite, Anti-Atlas, Morocco. *Precambrian Res.* 138 (3), 225–234.

Aldanmaz, E., 2012. Trace element geochemistry of primary mantle minerals in spinel-peridotites from polygenetic MOR-SSZ suites of SW Turkey: constraints from an LA-ICP-MS study and implications for mantle metasomatism. *Geol. J.* 47 (1), 59–76.

Allen, D.E., Seyfried Jr., W., 2003. Compositional controls on vent fluids from ultramafic-hosted hydrothermal systems at mid-ocean ridges: an experimental study at 400 °C, 500 bars. *Geochim. Cosmochim. Acta* 67 (8), 1531–1542.

Alt, J.C., Shanks, W.C., 1998. Sulfur in serpentized oceanic peridotites: serpentization processes and microbial sulfate reduction. *J. Geophys. Res. Solid Earth* 103 (B5), 9917–9929.

Alt, J.C., Shanks, W.C., Bach, W., Paulick, H., Garrido, C.J., Beaudoin, G., 2007. Hydrothermal alteration and microbial sulfate reduction in peridotite and gabbro exposed by detachment faulting at the Mid-Atlantic Ridge, 15°20'N (ODP Leg 209): a sulfur and oxygen isotope study. *Geochim. Geophys. Geosyst.* 8 (8), Q08002.

Arai, S., 1992. Chemistry of chromian spinel in volcanic rocks as a potential guide to magma chemistry. *Mineral. Mag.* 56 (383), 173–184.

Bach, W., Garrido, C.J., Paulick, H., Harvey, J., Rosner, M., 2004. Seawater-peridotite interactions: first insights from ODP Leg 209, MAR 15°N. *Geochem. Geophys. Geosyst.* 5 (9), Q09F26.

Bach, W., Paulick, H., Garrido, C.J., Ildefonse, B., Meurer, W.P., Humphris, S.E., 2006. Unraveling the sequence of serpentization reactions: petrography, mineral chemistry, and petrophysics of serpentinites from MAR 15°N (ODP Leg 209, Site 1274). *Geophys. Res. Lett.* 33 (13), L13306.

Barnes, S.J., 2000. Chromite in komatiites, II. Modification during greenschist to mid-amphibolite facies metamorphism. *J. Petrol.* 41 (3), 387.

Barnes, S.J., Roeder, P.L., 2001. The range of spinel compositions in terrestrial mafic and ultramafic rocks. *J. Petrol.* 42 (12), 2279.

Bazylev, B.A., Zakariadze, G., Zhelyazkova-Panayotova, M., Kolcheva, K., Oberhaensli, R., Solov'eva, N., 1999. Petrology of ultramafic rocks from the ophiolite association in the crystalline basement of the Rhodope massif. *Petroleum* 7, 192–211.

Bliss, N., MacLean, W., 1975. The paragenesis of zoned chromite from central Manitoba. *Geochim. Cosmochim. Acta* 39 (6), 973–990.

Bonev, N., 2006. Cenozoic tectonic evolution of the Eastern Rhodope massif (Bulgaria): basement structure and kinematics of syn- to post-collisional extensional deformation. In: Dilek, Y., Paulides, S. (Eds.), *Mediterranean Region and Asia. Geol. Soc. Am. Spec. Paper* 49, pp. 211–235.

Bonev, N., Peychev, K., Nizamova, D., 2006. MOR- vs. SSZ-origin of metamorphic rocks in the upper high-grade basement unit of the eastern Rhodope: geochemical diversity and tectonic significance. *Proceedings of Annual Conference of the Bulgarian Geological Society, Geosciences* 2006, pp. 181–184.

Burkhardt, D.J.M., 1993. Accessory chromium spinels: their coexistence and alteration in serpentinites. *Geochim. Cosmochim. Acta* 57 (6), 1297–1306.

Candia, M., Gaspar, J., 1997. Chromian spinels in metamorphosed ultramafic rocks from Mangabal I and II complexes, Goiás, Brazil. *Mineral. Petrol.* 60 (1), 27–40.

Cassard, D., Nicolas, A., Rabinovitch, M., Moutte, J., Leblanc, M., Prinzhofer, A., 1981. Structural classification of chromite pods in southern New Caledonia. *Econ. Geol.* 76 (4), 805–831.

Daieva, L., Haydoutov, I., Pristavova, S., 2007. Geochemical correlation of metabasic rocks from Central and East Rhodopes, Bulgaria. *Geochim. Mineral. Petrol.* 45, 109–118.

Dare, S.A.S., Pearce, J.A., McDonald, I., Styles, M.T., 2009. Tectonic discrimination of peridotites using FO_2 -Cr# and Ga-Ti- Fe^{III} systematics in chrome-spinel. *Chem. Geol.* 261 (3–4), 199–216.

Dick, H.J.B., Bullen, T., 1984. Chromian spinel as a petrogenetic indicator in abyssal and alpine-type peridotites and spatially associated lavas. *Contrib. Mineral. Petrol.* 86 (1), 54–76.

Droop, G., 1987. A general equation for estimating Fe_3 concentrations in ferromagnesian silicates and oxides from microprobe analyses, using stoichiometric criteria. *Mineral. Mag.* 51 (361), 431–435.

Evans, B.W., Frost, B.R., 1975. Chrome-spinel in progressive metamorphism—a preliminary analysis. *Geochim. Cosmochim. Acta* 39 (6–7), 959–972.

Frost, B.R., 1991. Stability of oxide minerals in metamorphic rocks. In: Lindsley, H.R. (Ed.), *Oxide Minerals: Petrologic and Magmatic Significance*. Mineral. Soc. Am. Rev. Mineral 25, pp. 469–487.

Gao, S., Liu, X., Yuan, H., Hattendorf, B., Günther, D., Chen, L., Hu, S., 2002. Determination of forty two major and trace elements in USGS and NIST SRM glasses by laser ablation-inductively coupled plasma-mass spectrometry. *Geostand. Newslett.* 26 (2), 181–196.

Georgiev, V., 2006. Tertiary domes and depressions in the Rhodope massif. *Proceedings of Annual Conference of the Bulgarian Geological Society, Geosciences* 2006, pp. 106–109.

Gervilla, F., Padrón-Navarta, J., Kerestedjian, T., Sergeeva, I., González-Jiménez, J., Fanlo, I., 2012. Formation of ferrian chromite in podiform chromitites from the Golyamo Kamenyane serpentinite, Eastern Rhodopes, SE Bulgaria: a two-stage process. *Contrib. Mineral. Petrol.* 164, 1–15.

González-Jiménez, J.M., Kerestedjian, T., Proenza Fernández, J.A., Gervilla Linares, F., 2009. Metamorphism on chromite ores from the Dobromirts ultramafic massif, Rhodope Mountains (SE Bulgaria). *Geol. Acta* 7 (4), 413–429.

González-Jiménez, J.M., Augé, T., Gervilla, F., Baily, L., Proenza, J.A., Griffin, W.L., 2011. Mineralogy and geochemistry of platinum-rich chromitites from the mantle–crust transition zone at Ouen Islad, New Caledonia Ophiolite. *Can. Mineral.* 49 (6), 1549–1569.

González-Jiménez, J.M., Locmelis, M., Belousova, E., Griffin, W.L., Gervilla, F., Kerestedjian, T.N., Pearson, N.J., Sergeeva, I., 2013. Genesis and tectonic implications of podiform chromitites in the metamorphosed Ultramafic Massif of Dobromirts (Bulgaria). *Gondwana Res.* <http://dx.doi.org/10.1016/j.gr.2013.09.020>.

González-Jiménez, J.M., Griffin, W.L., Gervilla, F., Proenza, J.A., O'Reilly, S.Y., Pearson, N.J., 2014. Chromitites in ophiolites: how, where, when, why? Part II. The crystallization of chromitites. *Lithos* 189, 140–158.

Grigori, G., Merlini, A., 2012. Chromite alteration processes within Vourinos ophiolite. *Int. J. Earth Sci.* 101 (6), 1523–1533.

Griffin, W., O'Reilly, S.Y., Afonso, J.C., Begg, G., 2009. The composition and evolution of lithospheric mantle: a re-evaluation and its tectonic implications. *J. Petrol.* 50 (7), 1185–1204.

Haydoutov, I., Kolcheva, K., Daieva, L., Savov, I., 2001. Island-arc origin of the neoproterozoic variegated formations from the east Rhodopes (Avren synform and Bela Reka antiform), Bulgaria. *EUROPROBE Meeting, METU, Ankara, Abs. 1*, pp. 31–32.

Haydoutov, I., Kolcheva, K., Daieva, L., Savov, I., Carrigan, C., 2004. Island arc origin of the variegated formations from the east Rhodope, Bulgaria—implications for the evolution of the Rhodope massif. *Ophioliti* 29 (2), 145–157.

Irvine, T., 1967. Chromian spinel as a petrogenetic indicator: part 2. Petrologic applications. *Can. J. Earth Sci.* 4 (1), 71–103.

Jan, M.Q., Windley, B.F., 1990. Chromian spinel-silicate chemistry in ultramafic rocks of the Jijal complex, Northwest Pakistan. *J. Petrol.* 31 (3), 667–715.

Janák, M., Froitzheim, N., Georgiev, N., Nagel, T., Sarov, S., 2011. P-T evolution of kyanite eclogite from the Pirin Mountains (SW Bulgaria): implications for the Rhodope UHP Metamorphic Complex. *J. Metamorph. Geol.* 29 (3), 317–332.

Kamenetsky, V.S., Crawford, A.J., Meffre, S., 2001. Factors controlling chemistry of magmatic spinel: an empirical study of associated olivine, Cr-spinel and melt inclusions from primitive rocks. *J. Petrol.* 42 (4), 655–671.

Kimball, K.L., 1990. Effects of hydrothermal alteration on the composition of chromian spinels. *Contrib. Mineral. Petrol.* 105, 337–346.

Kolcheva, K., Eskenazy, G., 1988. Geochemistry of metaecligites from the central and eastern Rhodope Mts (Bulgaria). *Geol. Balc.* 18 (5), 61–78.

Kolcheva, K., Haydoutov, I., Daieva, L., 2000. Dismembered ultramafic ophiolites from the Avren synform, Eastern Rhodopes. *Geochem. Mineral. Petrol.* 37, 25–38.

Kolkovski, B., Petrov, P., Dobrev, S., 2003. Hydrothermal ore-bearing features of igneous intrusive complexes. *Geol. Geophys.* 46 (1), 65–76.

Kozhukharov, D., Kozhukharova, E., Papanikolaou, D., 1988. Precambrian in the Rhodope massif. In: Zoubek, V. (Ed.), *Precambrian in Younger Fold Belts: European Variscides*, 851

852 the Carpathians, and Balkans. International Geological Correlation Programme, Project
853 22. Wiley, Chichester, pp. 773–778.

854 Leblanc, M., Nicolas, A., 1992. Ophiolitic chromitites. *Int. Geol. Rev.* 34 (7), 653–686.

855 Leblanc, M., Dupuy, C., Cassard, D., Moutte, J., Nicolas, A., Prinzhofer, A., Rabinovitch, M.,
856 Routhier, P., 1980. Essai sur la genèse des corps podiformes de chromite dans les pé-
857 ridotites ophiolitiques de Nouvelle-Calédonie et de Méditerranée orientale. In:
858 Panayiotou, A. (Ed.), Ophiolites: Proceedings of the International Ophiolite Symposium,
859 Nicosia, Cyprus, 1979. *Geol. Surv. Dep. Nicosia, Cyprus*, pp. 692–701.

860 Locmelis, M., Pearson, N.J., Barnes, S.J., Fiorentini, M.L., 2011. Ruthenium in komatiitic
861 chromite. *Geochim. Cosmochim. Acta* 75, 3645–3661.

862 LoferSKI, J.P., 1986. Petrology of metamorphosed chromite-bearing ultramafic rocks from
863 the Red Lodge District. *USGS Bull.*, Professional Paper 44.

864 Mellini, M., Rumori, C., Viti, C., 2005. Hydrothermally reset magmatic spinels in retrograde
865 serpentinites: formation of “ferritchromit” rims and chlorite aureoles. *Contrib. Miner-
866 al. Petrol.* 149 (3), 266–275.

867 Merlini, A., Grieco, G., Diella, V., 2009. Ferrichromite and chromian-chlorite formation in
868 mélange-hosted Kalkan chromitite (Southern Urals, Russia). *Am. Mineral.* 94 (10),
869 1459–1467.

870 Mposkos, E., 2002. Petrology of the ultra-high pressure metamorphic Kimi complex in
871 Rhodope (NE Greece): a new insight into the Alpine geodynamic evolution of the
872 Rhodope. *Bull. Geol. Soc. Greece* 34, 2169–2188.

873 Mposkos, E., Krohe, A., 2000. Petrological and structural evolution of continental high
874 pressure (HP) metamorphic rocks in the Alpine Rhodope Domain (N. Greece). In:
875 Panayides, I., Xenopoulos, C., Malpas, J. (Eds.), Proceedings of the 3rd International
876 Conference on the Geology of the Eastern Mediterranean (Nicosia, Cyprus). *Geol.
877 Surv. Cyprus*, pp. 221–232.

878 Mposkos, E., Krohe, A., 2006. Pressure–temperature–deformation paths of closely associated
879 ultra-high-pressure (diamond-bearing) crustal and mantle rocks of the Kimi complex: implications for the tectonic history of the Rhodope Mountains, northern
880 Greece. *Can. J. Earth Sci.* 43 (12), 1755–1776.

882 Mposkos, E., Baziotis, I., Proyer, A., 2011. Pressure–temperature evolution of eclogites
883 from the Kechros complex in the Eastern Rhodope (NE Greece). *Int. J. Earth Sci.*
884 101 (4), 973–996.

885 Mukherjee, R., Mondal, S.K., Rosing, M.T., Frei, R., 2010. Compositional variations in the
886 Mesoarchean chromites of the Nuggihalli schist belt, Western Dharwar Craton
887 (India): potential parental melts and implications for tectonic setting. *Contrib. Mineral.
888 Petrol.* 160 (6), 865–885.

889 Norman, M., Pearson, N., Sharma, A., Griffin, W., 1996. Quantitative analysis of trace ele-
890 ments in geological materials by laser ablation ICPMS: instrumental operating condi-
891 tions and calibration values of NIST glasses. *Geostand. Newslett.* 20 (2), 247–261.

892 Olobaniyi, S.B., Mücke, A., 2011. Chemical composition of chromite and intergrown
893 chlorite in metamorphosed ultramafic rocks (serpentinite and talc schist) of
894 the Ebge-Isanlu schist belt, southwest Nigeria: genetic implications. *J. Min.
895 Geol.* 47 (2), 115–134.

895 Pagé, P., Barnes, S.J., 2009. Using trace elements in chromites to constrain the origin of
896 podiform chromitites in the Thetford Mines ophiolite, Québec, Canada. *Econ. Geol.*
897 104 (7), 997–1018.

898 Proenza, J., Ortega-Gutiérrez, F., Camprubí, A., Tritlla, J., Elías-Herrera, M., Reyes-Salas, M.,
899 2004. Paleozoic serpentinite-enclosed chromitites from Tehuitzingo (Acatlán Com-
900 plex, southern Mexico): a petrological and mineralogical study. *J. S. Am. Earth Sci.*
901 16 (8), 649–666.

902 Proenza, J., Zaccarini, F., Escayola, M., Cábana, C., Schalamuk, A., Garuti, G., 2008. Compo-
903 sition and textures of chromite and platinum-group minerals in chromitites of the
904 western ophiolitic belt from Pampean Ranges of Córdoba, Argentina. *Ore Geol. Rev.*
905 33 (1), 32–48.

906 Rollinson, H., 2008. The geochemistry of mantle chromitites from the northern part of the
907 Oman ophiolite: inferred parental melt compositions. *Contrib. Mineral. Petrol.* 156
908 (3), 273–288.

909 Rollinson, H., Appel, P.W.U., Frei, R., 2002. A metamorphosed, early Archaean chromitite
910 from west Greenland: implications for the genesis of Archaean anorthositic
911 chromitites. *J. Petrol.* 43 (11), 2143–2170.

912 Sack, R.O., Ghiorsu, M.S., 1991. Chromian spinels as petrogenetic indicators – thermody-
913 namics and petrological applications. *Am. Mineral.* 76 (5–6), 827–847.

914 Satsukawa, T., González-Jiménez, J.M., Colás, V., Griffin, W.L., Piazolo, S., O'Reilly, S.Y.,
915 Gervilla, F., Fanlo, I., 2014. Fluid-induced deformation in chromite during metamor-
916 phism. *Proceedings of 6th Orogenic Lherzolite Conference, Marrakech 2014.*

917 Singh, A.K., Singh, R.B., 2013. Genetic implications of Zn- and Mn-rich Cr-spinels in
918 serpentinites of the Tidding Suture Zone, eastern Himalaya, NE India. *Geol. J.* 48 (1),
919 22–38.

920 Stowe, C.W., 1994. Compositions and tectonic settings of chromite deposits through time.
921 *Econ. Geol.* 89 (3), 528–546.

922 Wylie, A.G., Candela, P.A., Burke, T.M., 1987. Compositional zoning in unusual Zn-rich
923 chromite from the Sykesville district of Maryland and its bearing on the origin of
924 “ferritchromit”. *Am. Mineral.* 72 (3–4), 413–422.

925 Zhou, M., Robinson, P.T., 1994. High-Cr and high-Al podiform chromitites, Western China:
926 relationship to partial melting and melt/rock reaction in the upper mantle. *Int. Geol.
927 Rev.* 36 (7), 678–686.

928